Title

Surface Lin28A expression consistent with cellular stress parallels indicators of senescence

Journal

Cardiovascular Research, 119(3)

ISSN

1015-5007

Authors

Broughton, Kathleen

Esquer, Carolina

Echeagaray, Oscar

et al.

Publication Date

2023-05-02

DOI

10.1093/cvr/cvac122

Peer reviewed

ESC European Society of Cardiology

Cardiovascular Research (2022) **00**, 1–16
https://doi.org/10.1093/cvr/cvac122

Surface Lin28A expression consistent with cellular stress parallels indicators of senescence

Kathleen Broughton, Carolina Esquer, Oscar Echeagaray, Fareheh Firouzi, Grant Shain, David Ebeid, Megan Monsanto, Dena Yaareb, Leila Golgolab, Natalie Gude, and Mark A. Sussman *

San Diego State University Heart Institute and Department of Biology, San Diego State University, 5500 Campanile Drive, San Diego, CA 92182, USA

Received 4 November 2021; revised 3 June 2022; accepted 26 June 2022; online publish-ahead-of-print 26 July 2022

Time of primary review: 70 days

Aims Declining cellular functional capacity resulting from stress or ageing is a primary contributor to impairment of myocardial performance. Molecular pathway regulation of biological processes in cardiac interstitial cells (CICs) is pivotal in stress and ageing responses. Altered localization of the RNA-binding protein Lin28A has been reported in response to environmental stress, but the role of Lin28A in response to stress in CICs has not been explored. Surface Lin28A redistribution is indicative of stress response in CIC associated with ageing and senescence.

Methods and results Localization of Lin28A was assessed by multiple experimental analyses and treatment conditions and correlated to oxidative stress, senescence, and ploidy in adult murine CICs. Surface Lin28A expression is present on 5% of fresh CICs and maintained through Passage 2, increasing to 21% in hyperoxic conditions but lowered to 14% in physiologic normoxia. Surface Lin28A is coincident with elevated senescence marker p16 and beta-galactosidase (β-gal) expression in CICs expanded in hyperoxia, and also increases with polyploidization and binucleation of CICs regardless of oxygen culture. Transcriptional profiling of CICs using single-cell RNA-Seq reveals up-regulation of pathways associated with oxidative stress in CICs exhibiting surface Lin28A. Induction of surface Lin28A by oxidative stress is blunted by treatment of cells with the antioxidant Trolox in a dose-dependent manner, with 300 μM Trolox exposure maintaining characteristics of freshly isolated CICs possessing low expression of surface Lin28A and β-gal with predominantly diploid content.

Conclusion Surface Lin28A is a marker of environmental oxidative stress in CICs and antioxidant treatment antagonizes this phenotype. The biological significance of Lin28 surface expression and consequences for myocardial responses may provide important insights regarding mitigation of cardiac stress and ageing.

* Corresponding author. Tel: +1 619 594 8632; fax: +1 619 594 8635, E-mail: heartman4ever@icloud.com

Graphical Abstract

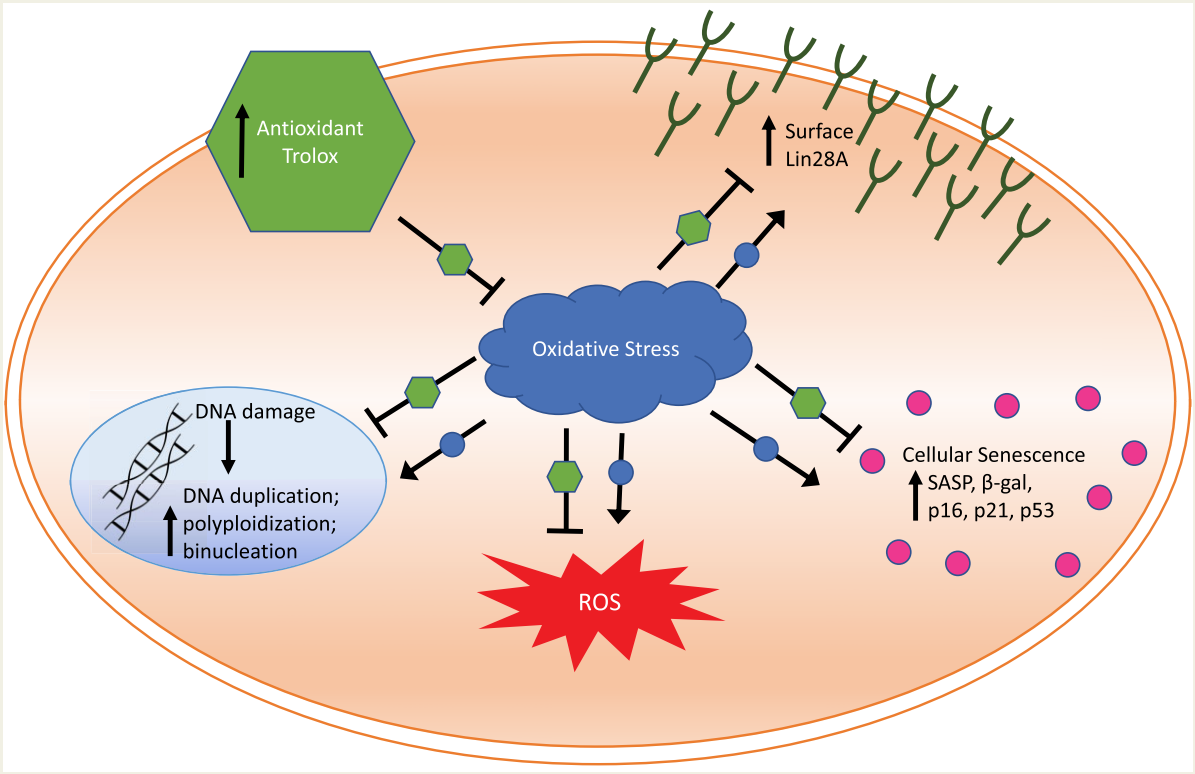

Keywords Lin28A • Surface marker • Senescence • Oxidative stress • Ploidy

1. Introduction

Cardiovascular disease (CVD) prevalence in adults over 20 years old affects nearly half of the global population.[1] Although many CVDs can be managed after diagnosis, congestive heart failure (HF) is a chronic condition that develops with time and biological ageing. HF has a particularly poor prognosis with a 5-year mortality rate of 68.7% and average survival of 2.4 after diagnosis in older adults.[2] HF is the most common cause of hospitalization and leading cause of death in older adults within the USA.[1] These statistics are sobering and, when considered in the aggregate, are a driving force behind cardiovascular research to blunt deterioration and repair the myocardium. Ageing remains a primary causal factor in loss of cardiac structure, function, and reparative capacity.[3] Delineating fundamental biological processes of the ageing heart will advance prevention and management of HF.

Compensatory changes in response to normal biological ageing of the heart lead to decreased tissue compliance, impaired contractile reserve, and replacement fibrosis in the wake of cumulative myocyte losses. Cardiac interstitial cells (CICs) perform a critical role in the ageing process through regulation of myocardial structure, interaction with cardiomyocytes, and ongoing contribution to cellular renewal throughout lifespan. Indeed, CIC activity mediates homeostasis and regulates phenotypic alterations of myocardial structure that typify the ageing heart.[3–5] Although the heart is characterized by barely perceptible myocyte turnover in adulthood, CIC proliferative capacity is retained throughout life even as senescence markers accumulate.[6,7] Interventional approaches to slow, stop, or reverse ageing cardiomyopathy depend upon understanding regulatory mechanisms, influencing CIC proliferation, senescence, and polyploidization.[8] Mitigation of the ageing process depends upon greater understanding of stress and senescence markers that arise within and identify cells with compromised biological properties. Our laboratory has been investigating biological responses of the CIC population to acute stress and ageing. Evidence has been accumulating to demonstrate that RNA-binding proteins such as Lin28 and nucleolin are involved in cellular stress responses.[9–11] Lin28 has been identified as a molecule transported to the cell surface in extracellular vesicles to exert biological effects[12] and is associated with localization in stress granules and p-bodies.[13] Consistent with these observations, we found Lin28 expression on the cell surface as well as intracellularly. Detailed characterization revealed association between surface Lin28 (Lin28A^{S+}) expression, oxidative stress, and acquisition of ageing hallmarks such as beta-galactosidase (β-gal) and polyploidization.

Lin28A is an RNA-binding protein typically associated with stem-cell pluripotent state that has recently garnered attention as a regulator of proliferation, metabolism, and regenerative potential.[14] Lin28/let-7 antagonism controls development, stem-cell biology, ageing, and metabolism through Lin28-mediated repression of heterochronic *let-7* miRNA biogenesis that, not coincidentally, reciprocally represses Lin28 expression.[15–20] However, the myocardial biology of Lin28 is relatively unstudied. Several references have linked *let-7* activity to cardiomyopathic

effects.[21–25] Specifically, inhibition of *let*-7 attenuates remodelling and improves haemodynamic function after myocardial infarction and ischaemia-reperfusion injury.[24–27] Interestingly, one report links hypoxia-induced Lin28 up-regulation in cardiomyocytes (but not cardiac fibroblasts) to increased apoptotic susceptibility that can be blunted by restoration of *let*-7*g*.[28] Inhibition of *let*-7 is also associated with postnatal hypertrophy in neonatal rats.[29] Such superficially divergent observations in the myocardial context are likely reconciled by cell type–specific Lin28 functional consequences. In the case of cardiomyocytes, Lin28 up-regulation could mediate switching from aerobic to glycolytic metabolism that is a hallmark of HF and pathologic injury rather than serving as a molecular mechanism for repair or regeneration. Collectively, these findings suggest the Lin28/*let*-7 axis can be either beneficial or maladaptive depending upon timing, cell type, and duration of temporal expression as expected for a powerful heterochronic molecular regulator.[14,19,30,31] Lin28 in the context of myocardial ageing and chronic stress has not been previously assessed.

Collective biological actions of Lin28 suggest a potential role for influencing ageing and, consequently, ploidy state of the CIC population. Fluidity of cellular ploidy in the cardiovascular system prompts diverse interpretations as to the role for polyploid cells in adaptation, ageing, and the healing process.[32] Prior research by our group revealed rodent c-kit+ CICs (cCICs), compared with large mammal (human, swine, and feline) cCICs, uniquely respond to environmental stress of cell culturing in 21% oxygen through tetraploidization.[8] This aligns with the dogma that polyploidy of the myocardium increases with age as cardiomyocytes accumulate elevated DNA content from endomitosis (multinucleation) or endoreplication (polyploid nuclei). Frequency of higher cardiomyocyte ploidy levels also naturally increase in environmental stress, such as diabetic compared with normal mice.[33] Ploidy plasticity also occurs, such as the human heart responding to infarction by reduction of tetraploid cells and increased number of nuclei.[34] Polyploidization and increased DNA content also occurs in end-stage cardiomyopathies.[35] Ploidy reduction also occurs in response to alleviation of chronic environmental stress in the human heart following left ventricle assist device (LVAD) implantation.[36] Vascular smooth muscle cells exist in multiple ploidy states provoked by hypertension, oxidative stress, or senescence.[37,38] Although cardiomyocytes exist in conjunction with an extensive CIC population that regulates function and response to pathologic damage or stress,[39,40] the significance of ploidy state in CICs remains an understudied and underappreciated population contributing to the health and function of the myocardium in ageing, environmental stress, and disease.

Our studies reveal a novel role for Lin28A in CICs corresponding to surface expression in response to oxidative stress conditions such as those typically present in damaged or aged myocardium. The relationship of Lin28A^{S+} to stress response of CICs including polyploidization, reduced proliferation, and senescence reveals surface Lin28A as a novel marker of cellular senescence. Lin28A^{S+} expression serves as a phenotypic marker for CICs possessing characteristics of aged cells and the expression of surface Lin28A in conjunction with oxidative stress in this study advances understanding of molecular events in the ageing myocardium.

2. Methods

2.1 Human tissue

Samples of deidentified human heart were obtained from the National Disease Research Interchange (NDRI; http://ndriresource.org) and the Cooperative Human Tissue Network (CHTN; https://www.chtn.org), including both paraffin-embedded tissue blocks for microscopy and snap-frozen tissue chunks for western blot. Samples vary in age and ethnicity as determined by sample availability and each sample was determined as non-pathological (normal function) heart tissue by the NDRI and CHTN.

2.2 Animal experiments

All animal protocols were approved by the Institutional Animal Care and Use Committee of San Diego State University and conform to the *Guide for the Care and Use of Laboratory Animals* published by the US National Institutes of Health. Adult mice aged 6 months from gender-matched mice of the same strain (FVB) were used for the study with the exception of the Canto flow cytometry ageing experiment that used available young (3 months) and old (24 months) C57BL/6 mice.

2.3 Isolation and culture of adult mouse cardiac interstitial cells

Cardiac interstitial cells were isolated from adult mice according to the standard laboratory protocol as previously described.[8] Briefly, mice were anaesthetized with a single dose intraperitoneal injection of 0.5 mg/mL xylazine(AnaSed, Santa Cruz Laboratories, Santa Cruz, CA, USA)/12 mg/mL ketamine(VetaKet, Akorn Pharmaceuticals, Lake Forest, IL, USA) solution in a weight-dependent manner along with heparin (100 IU/kg; Sigma-Aldrich, Burlington, MA, USA; H3393) to prevent blood clots. Mice were sacrificed ≈5–10 min later using cervical dislocation procedure. The chest was opened, and the aortic arch was exposed. Curved forceps were used to push 4-0 suture underneath the aorta. A small incision was made at the aortic branch and a cannula was inserted into the aorta then tied securely with suture. The cannula was attached to a Langendorff apparatus, and the heart was perfused until all blood was cleared. The heart was then digested using buffer containing Collagenase II (230 IU/mL; (Worthington Biochemical Corporation, Lakewood, NJ, USA); LS004147) for 12 min. Hearts were gently teased apart using forceps and triturated until no large tissue remained. The cell suspension underwent filtering through a 100 μm filter and centrifuged (10 min, 600 *g*, 4°C) followed by filtering through a 40 μm filter and centrifuged (10 min, 600 *g*, 4°C) in 5% foetal bovine serum in phosphate buffered saline (PBS). Total CICs were plated in DMEM/F-12-based media as previously described[8] and were maintained with media changes every 3 days and outgrowth replating at approximately 70% confluency to Passage 2 in either 1 or 21% oxygen. Fresh isolate experiments were performed immediately after filtering step.

2.4 Immunohistochemistry

Mice were anaesthetized as described above and the heart was retroperfused, removed from the animal, and fixed in 10% formalin overnight. Tissue was then treated with 70% ethanol prior to paraffin embedding using a Leica eASP300 enclosed tissue processor (Leica Biosystems, Buffalo Grove, IL, USA). Paraffin processed tissues were cut into 5 μ section and slide mounted using an HM 355S Automatic Microtome (Thermo Fisher Scientific, Waltham, MA, USA). Heart sections were deparaffinized and incubated with primary and secondary antibodies as previously described.[8] Primary antibody Lin28A (PA1-096; Thermo Fisher Scientific, Waltham, MA, USA) was applied 1:200, and p16 (1661; Santa Cruz Biotechnology, Dallas, TX, USA) 1:100 overnight in 4°C and secondary antibody 1:400 (Thermo Fisher Scientific, Waltham, MA, USA) antibodies for 1.5 h room temperature. The tissue

is then rinsed with PBS, DNA is stained with 1 nM 4′,6-diamidino-2-phenylindole (DAPI; Thermo Fisher Scientific, Waltham, MA, USA) 1:10 000 in PBS for 10 min and Vectashield mounting medium is applied (Vector Laboratories, Newark, CA, USA). Slides were visualized using a Leica TCS SP8 confocal microscope (Leica Microsystems, Wetzlar, Germany).

2.5 Immunocytochemistry

Total CICs were placed at a density of 10 000 per well of a two-chamber permanox slide and grown for 48 h. For Lin28 surface analysis, live cells were incubated with Lin28A (1:20) in wash buffer in the incubator for 30 min. Cells were washed and labelled with secondary antibody (1:50) in the incubator for 30 min. Cells were then fixed in 4% paraformaldehyde for 10 min at room temperature. Cells are then permeabilized using 0.03 M glycine for 5 min followed by 0.5% Triton-X 100/PBS for 10 min to reduce non-specific binding. Cells were blocked with 10% horse serum in PBS for 30 min at room temperature followed by primary antibody in 10% horse serum in PBS overnight at 4°C. The next day, cells were rinsed with PBS then labelled with secondary antibody and/or phalloidin in 10% horse serum in PBS for 45 min. Cells are then rinsed with PBS, DNA is stained with 1 nM DAPI (Thermo Fisher Scientific, Waltham, MA, USA) 1:10 000 in PBS for 5 min and Vectashield mounting medium is applied (Vector Laboratories, Newark, CA, USA). Slides were visualized using a Leica TCS SP8 confocal microscope.

2.6 Immunoblot

Cardiac interstitial cell samples were collected in 1X sodium dodecyl sulphate (SDS) sample buffer with protease and phosphatase inhibitors. Cell lysates were boiled for 10 min and stored at −80°C. Proteins were loaded into 4–12% Bis-Tris gel (Thermo Fisher Scientific, Waltham, MA, USA) and run in 1X MES SDS running buffer (Thermo Fisher Scientific, Waltham, MA, USA) at 150 V for 1.5 h on an electrophoresis apparatus (Invitrogen, Carlsbad, CA, USA). Separate proteins were transferred to a polyvinylidene difluoride membrane in 1X transfer buffer (Thermo Fisher Scientific, Waltham, MA, USA) then blocked with Odyssey blocking buffer (TBS; LI-COR, Lincoln, NE, USA) for 1 h. After blocking, membrane was incubated with primary antibody Lin28A (1:100) and GAPDH (1:200) in Odyssey blocking buffer at 4°C overnight. The next day, the membrane was washed with 1X TBST three times at 15 min, room temperature on an orbital rocker. The membrane was then incubated with secondary antibodies for Lin28A (1:500) and GAPDH (1:1000) in Odyssey blocking buffer for 1.5 h at room temperature on an orbital rocker followed by three washes of 1X TBST for 15 min a wash, room temperature on an orbital rocker. The membrane was then scanned using an Odyssey CLx (LI-COR, Lincoln, NE, USA).

2.7 Flow cytometry

To prepare CICs for flow cytometry using BDFACS Canto or Amnis ImageStream, approximately 50 000 cells were disassociated, suspended in media, then centrifuged at 200 g for 5 min at 22°C. For Lin28A surface analysis, live cells were suspended and incubated with Lin28A (1:20) in wash buffer (0.5% BSA/PBS) on ice for 30 min. For fresh isolate analysis using the BDFACS Canto, CICs were additionally labelled using Vybrant DyeCycle Ruby (Thermo Fisher Scientific, Waltham, MA, USA) as a means to gate viable CICs, since the cytometer does not offer visual analysis. Cells were washed and resuspended with secondary antibody (1:50) on ice for 30 min. Cells were either sorted or then fixed in 4% paraformaldehyde. Following fixation, cells were either incubated with senescence-associated β-gal according to manufacturer recommendations (CellEvent Senescence Green Flow Cytometry Assay; Thermo Fisher Scientific, Waltham, MA, USA), or with 1 nM DAPI at 1:20 000 for 10 min. Cells were washed and imaged with flow cytometry quantitation on a Luminex Amnis ImageStream using the Amnis Inspire software (Luminex Corporation, Austin, TX, USA). Amnis data were analysed using Amnis Ideas software (Luminex Corporation, Austin, TX, USA) and BDFACS Canto (Becton Dickinson and Company, Franklin Lakes, NJ, USA) data were analysed using FlowJo (BD, Ashland, OR, USA).

2.8 Hydrogen peroxide analysis

Hydrogen peroxide is a known reagent to cause oxidative stress and is a technique commonly used by our team.[41] To confirm surface, Lin28A is involved in a response to oxidative stress, Passage 2 CICs that were maintained in 1% oxygen were plated in a 6-well plate at a density of 50 000 cells per well in regular media overnight. After 24 h, cells were then washed, and media was changed to either regular media or low serum without growth supplements. After another 20 h, samples in low serum without growth supplements had media changed to low serum without growth supplements and 300 μM hydrogen peroxide for 4 h. Live cells were then rinsed, suspended, and incubated with Lin28A (1:20) in wash buffer (0.5% BSA/PBS) on ice for 30 min then washed and resuspended with secondary antibody (1:50) on ice for 30 min. Cells were washed and imaged with flow cytometry quantitation on a Luminex Amnis ImageStream using the Amnis Inspire software. Data were analysed using Amnis Ideas software (Luminex).

2.9 Reactive oxygen species and ROS/RNS analysis

Reactive oxygen species (ROS) and reactive nitrogen species (RNS) are a contributing factor leading to accelerated ageing[42–46] and are involved in cardiac reperfusion injury and reperfusion alteration of mitochondrial and tissue function.[47,48] To measure ROS and ROS/RNS activity, cells from 1 and 21% oxygen content were plated at Passage 1 split on a 96-well plate at a density of 500 cells per well and left to settle overnight. The following day, cells were stained with a cell-permeable fluorogenic probe 2′,7′-dichlorodihydrofluorescin diacetate (DCFH-DA), which is diffused into cells, oxidized by ROS, and produces a fluorescence intensity proportional to ROS within the cell cytosol, as described by manufacturers (Cell Bio Labs, San Diego, CA, USA). Similarly, ROS/RNS, to detect total free radical presence, can be measured in a similar fashion with the probe DCFH-DiOxyQ (Cell Bio Labs, San Diego, CA, USA). Assays were performed according to manufacturer recommendations and measurements were taken using a spectrometer.

2.10 Antioxidant treatment

Total CICs were isolated from 6-month-old FVB mice and were immediately plated at the same density in either regular media or regular media with Trolox (Sigma-Aldrich, Saint Louis, MO, USA) in a dose-dependent manner. Media, with or without Trolox, was changed and cells were expanded according to standard protocol for two passages, with replating at the same density. At Passage 2, total CICs were then studied for oxidative stress-related properties including proliferation, cell size, surface Lin28A, senescence-associated β-gal, ploidy, and nucleation.

2.11 Single-cell RNA-Seq

Freshly isolated single-cell suspensions were loaded on a Chromium™ Controller (10x Genomics, Pleasanton, CA, USA) and single-cell RNA-Seq (scRNA-Seq) libraries were prepared using Chromium™ Single-Cell 3′ Library & Gel Bead Kit v3 (10x Genomics, Pleasanton, CA, USA; Item 1000075) following manufacturer's protocol. Concentration and fragment size distribution of each library were tested with Bioanalyzer (Agilent High Sensitivity DNA Kit, Cat. #5067-4626; average library size: 450–490 bp). The sequencing libraries were quantified by quantitative PCR (KAPA Biosystems Library Quantification Kit for Illumina platforms P/N KK4824) and Qubit 3.0 with dsDNA HS Assay Kit (Thermo Fisher Scientific, Waltham, MA, USA). Sequencing libraries were submitted to the UCSD IGM Genomics Core for sequencing (NovaSeq 6000, Illumina, San Diego, CA, USA).

2.12 Single-cell selection and quality control

The raw data were processed with the Cell Ranger pipeline (10X Genomics, Pleasanton, CA, USA; version 3.0.1, SF 1). Sequencing reads were aligned to the 10x mouse genome mm10. Cells with fewer than 200 genes were filtered out to avoid inclusion of empty droplets in downstream analysis. Based on UMI and gene detection distribution droplets, multiplets were excluded using the Interquartile Range Rule (values over the third quartile and 1.5 the interquartile range are considered outliers). Cell with >15% of mitochondrial gene UMI count and genes detected in fewer than three cells were filtered out using Seurat R Package (v4.0.2).[49] The first eight principal components were found to be significant to perform dimensionality reduction. Preparations derived from Lin28 cell surface sorting yielded 7086 barcoded cells for analysis, from which 4334 corresponded to $Lin28^{S-}$, and 2752 corresponded to $Lin28^{S+}$(874 $Lin28^{S+}$/c-kit−, 1878 $Lin28^{S+}$/c-kit+). Final removal of unwanted sources of variation and batch effect corrections was performed using Seurat R Package (v4.0.2).[49]

2.13 Dimensionality reduction and unsupervised clustering

Approximately 2000 variable genes were selected based on their expression and dispersion. Prior dimensionality reduction, data were scaled to mean expression equal to 0 and variance across cells equal to 1. Principal component analysis (PCA) was performed on the scaled data as a linear dimensionality reduction approach. The first eight most significant principal components (PCs) were selected for non-linear dimensional reduction (PCA, t-distributed stochastic neighbor embedding (t-SNE), and Uniform Manifold Approximation and Projection (UMAP); see Supplementary material online, *Figure S8*) and unsupervised clustering using complementary methods, including supervised PC selection, Jackstraw statistical and heuristic approaches. Clusters were validated by concurrent expression of housekeeping genes (Gapdh, Actb, Rplp0, B2m, and Ywhaz; see Supplementary material online, *Figure S9*). Cell-type annotation of unsupervised clusters was based on cell known markers. Clusters not expressing canonical cell markers were classified using the clustifyr package[50] using the Tabula muris data as reference set for classification.[51]

2.14 Differential expression analysis

Differential expression analysis was done using Wilcoxon rank sum test and selecting for a threshold of 0.05 for an adjusted *P*-value and a log (FC) >0.25 was used to define statistically significant and differentially expressed genes (DEGs).

2.15 Gene ontology analysis

Gene ontology(GO) enrichment analysis for DEGs lists derived from Neonatal, LVAD, and Intermediate cells was performed using the enrichGO and compareCluster functions of clusterProfiler (3.16.1) R package.[52] GO terms were selected with *P*-value cut-off of 0.05 using BH method.

2.16 Statistical analyses

All data are expressed as mean ± standard error of mean. Each dot for each dot plot represents an experiment point, with at least three independent experiments for statistical analysis (western blot consisted of three independent blot runs with multiple samples per condition). Statistical analyses were performed within and between-group comparisons, Student's *t*-test, one- and two-way analysis of variance (ANOVA) were applied with Bonferroni post-test, when applicable using Graph Pad Prism v5.0 (GraphPad Software, La Jolla, CA, USA). A *P*-value of <0.05 was considered statistically significant ($^{*}P<0.05$, $^{**}P<0.01$, $^{***}P<0.001$).

3. Results

3.1 Lin28A is expressed in human and rodent cardiac tissue

Normal neonatal and adult ventricle cardiac tissues were immunolabelled for Lin28A, myosin light chain, connective tissue, and DNA. CICs and cardiomyocytes express Lin28A in adult normal and HF samples, whereas foetal tissue demonstrated fewer Lin28A-positive-stained cells (*Figure 1A*). Lin28A protein level was significantly increased in aged adult (1.445 ± 0.2767), compared with control neonatal (1.00 ± 0.1898) samples (*Figure 1B* and *C*; $^{***}P<0.001$). Heart tissue sections from adult mice showed comparable Lin28A immunoreactivity (*Figure 1D*). Total CICs were isolated from ventricle tissue of adult FVB mice of both male and female mice in four experiments, stained for surface Lin28A in fresh, live cells and sorted. Surface Lin28A expression between male (5.760 ± 2.916%) and female (4.393 ± 1.427%) samples showed no statistical differences (*Figure 1E*). Surface Lin28A ($Lin28A^{S+}$) frequency in freshly isolated CICs significantly increased in aged (52.68 ± 1.897%) samples vs. young (7.717 ± 1.711%) from C57BL/6 mice (*Figure 1F*; $^{***}P<0.0001$). Tissue sections reveal presence of $Lin28A^{S+}$ CICs in aged hearts frequently observed in clusters compared with young FVB mice by confocal microscopy (*Figure 1G*). Concurrently, $Lin28A^{S+}$ CICs were also positive for senescence marker p16 (*Figure 1H*). After infarction injury, a significant number of $Lin28A^{S+}$ CICs were present proximal to the injury and border zone distinct from the c-kit population (see Supplementary material online, *Figure S2*).

3.2 Oxidative stress promotes $Lin28A^{S+}$ expression together with CIC senescence phenotype

$Lin28A^{S+}$ expression was assessed relative to senescence-associated β-gal (β-gal^{+}) as well as cell area. Analyses were performed using initial isolates of CICs or descendants minimally expanded *in vitro* by two passages in either 1 or 21% O_2. Amnis ImageStream was used for flow

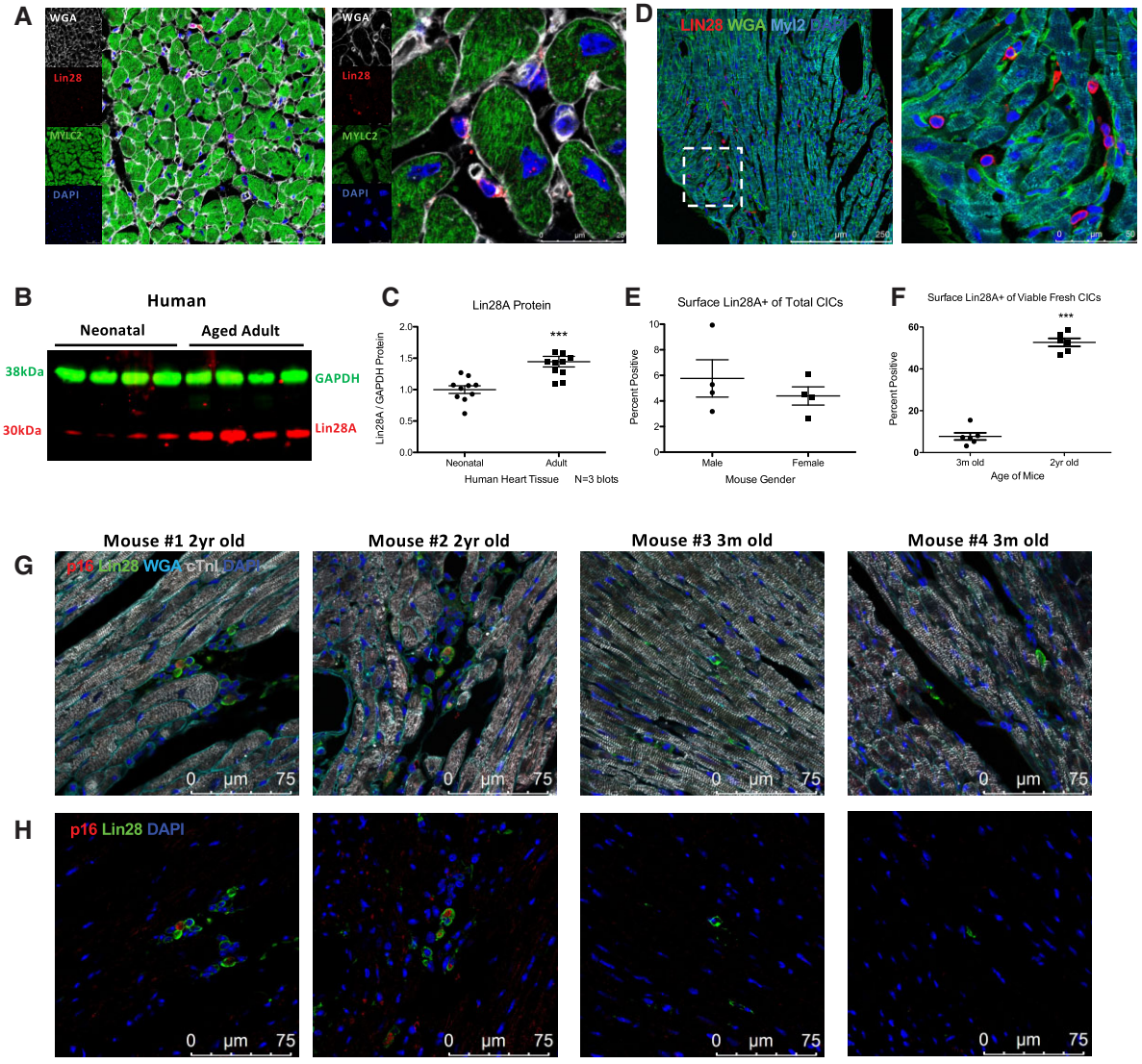

Figure 1 Lin28A is expressed in human and rodent cardiac tissue. (*A*) Adult human cardiac tissue demonstrating Lin28A is endogenous to both cardiomyocytes and CICs, as shown by immunohistochemistry stain. (*B*) Protein quantity of Lin28A is significantly increased in aged normal heart tissue compared with neonatal cardiac tissue. (*C*) Quantification of Lin28A, normalized to GAPDH, verifies aged human cardiac tissue has an increased amount of Lin28A protein compared with neonatal human cardiac tissue ($N = 3$ blots). (*D*) Adult FVB mouse cardiac tissue demonstrates Lin28A is endogenous to CICs, shown by immunohistochemistry stain. (*E*) Lin28A^{S+} is equally present in freshly isolated male and female FVB adult isolate CICs ($N = 3$). (*F*) Lin28A^{S+} positive freshly isolated CICs significantly increases in samples derived from aged relative to young C57BL/6 mice ($N = 6$). (*G*) Lin28A^{S+} positive CICs identified by confocal microscopy in cardiac sections from aged vs. young FVB mice. (*H*) Lin28A^{S+} positive CICs frequently are also positive for senescence marker p16 in aged vs. young FVB mice. Statistical significance (*$P < 0.05$, **$P < 0.01$, ***$P < 0.001$) was determined by *t*-test (*C*, *E*, *F*).

cytometry visualization of CIC phenotypic characteristics in population-based analyses (*Figure 2A*, see Supplementary material online, *Figure S3*). Immunocytochemistry demonstrates that CICs in 21% O_2 are larger, and more frequently, Lin28A^{S+} relative to smaller spindle-shaped Lin28A^{S-} CICs (*Figure 2B*). Oxidative stress increased frequency of Lin28A^{S+} or β-gal^{+} CICs expanded at 21% O_2 level (19.7 ± 2.4%) vs. cells at 1% O_2 (8.4 ± 1.8%) or freshly isolated CICs (4.5 ± 1.0%; *Figure 2C*; **$P < 0.01$). *In vitro* culture increased Lin28A^{S+} expression at 21% O_2 (21.1 ± 1.7%) vs. either 1% O_2 (14.1 ± 2.2%) or CICs direct from tissue without culture (4.4 ± 1.4%; *Figure 2D*; **$P < 0.01$). The role of oxidative stress in promotion of Lin28A^{S+} was confirmed by treatment with hydrogen peroxide (H_2O_2), which increased frequency of Lin28A^{S+} CICs when expanded in 1% oxygen (see Supplementary material online, *Figure S2*). Cell area of Lin28A^{S+} was consistently larger compared with Lin28A^{S-} CIC whether assessed using freshly isolated (734.5 ± 258 µm^2 vs. 324.6 ± 9.138 µm^2, respectively) or cells cultured under oxygen levels of 1% (1261 ± 439.7 µm^2 vs. 594.7 ± 55.7 µm^2, respectively) and 21% (1879 ± 182.7µm^2 vs. 844.1 ± 0.67.0 µm^2, respectively; *Figure 2E*; *$P < 0.05$). Similarly, β-gal^{+} CICs were more prevalent at 21% O_2 (17.78 ± 4.7%) relative to expansion in 1% O_2 (6.30 ± 3.7%) or in fresh isolates (1.640 ± 0.6398%; *Figure 2F*; **$P < 0.01$). Likewise, surface area of β-gal^{+} vs. β-gal^{-} CICs was highest in 21% O_2 (2050 ± 94.5 µm^2 vs. 601.0 ± 56.8µm^2), lower in 1% O_2 (1732 ± 330.8 µm^2 vs. 538.3 ± 44.4 µm^2), and lowest in fresh isolates (1256 ± 445.9 µm^2 vs. 328.0 ± 12.90 µm^2; *Figure 2G*; ***$P < 0.001$). Lin28A^{S+} CICs

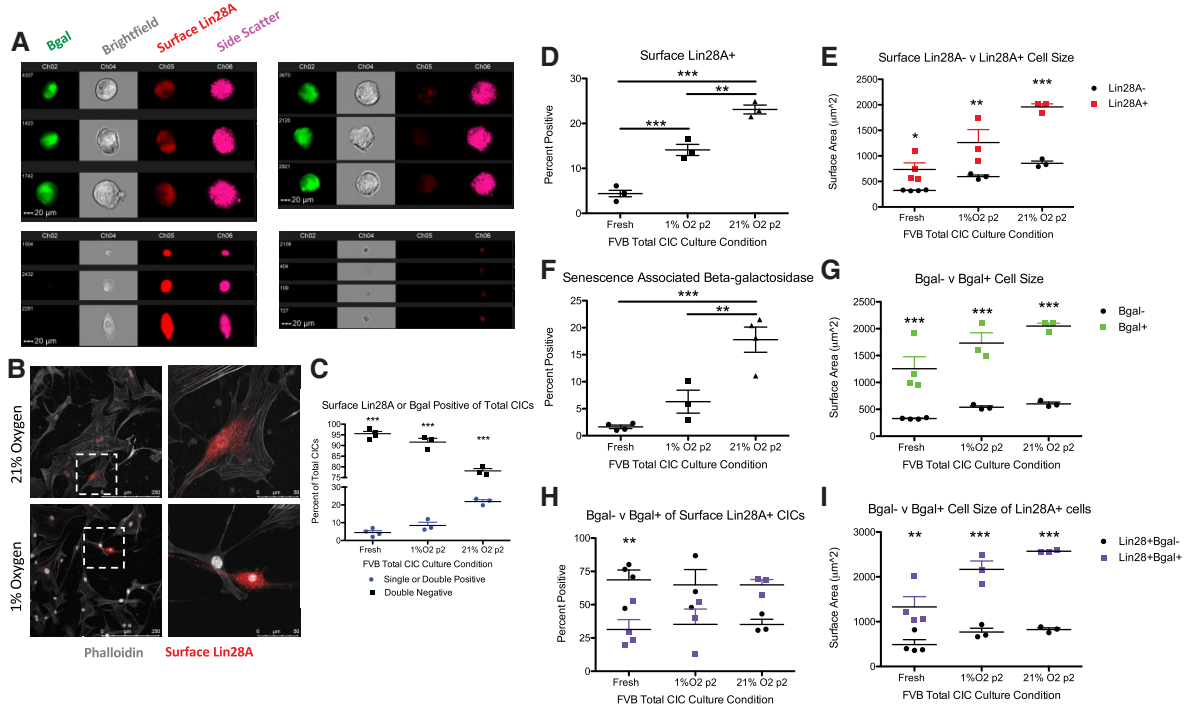

Figure 2 Oxidative stress promotes Lin28A^{S+} expression together with CIC senescence phenotype. (*A*) Amnis ImageStream flow cytometry was used to identify and count FVB total CICs for β-gal (Ch02), Brightfield (Ch04), Lin28A^{S} (Ch05), side scatter (Ch06), organized as Lin28A^{S+}/β-gal^{+} (top left), β-gal^{+} (top right) Lin28A^{S-} (bottom left), Lin28A^{S-}/β-gal^{-} (bottom right). (*B*) Immunocytochemistry of FVB total CICs Passage 2 stained for phalloidin and surface Lin28A. (*C*) Fresh isolate CICs are mostly Lin28A^{S-}/β-gal^{-}, compared with 1 and 21% O_2. (*D*) The frequency of Lin28A^{S+} CICs is significantly increased in higher O_2 culture. (*E*) The size of Lin28A^{S+} CICs is significantly larger compared with Lin28A^{S-} CICs, regardless of O_2 culture. (*F*) The frequency of β-gal^{+} CICs is significantly increased in higher O_2 culture. (*G*) The size of β-gal^{+} CICs is significantly larger compared with β-gal^{-} CICs, regardless of O_2 culture. (*H*) Of Lin28A^{S+} CICs, β-gal^{+} is more likely present in 21% O_2 culture. (*I*) Lin28A^{S+}/β-gal^{+} CICs are significantly larger in size, regardless of O_2 culture. Statistical significance (*$P < 0.05$, **$P < 0.01$, ***$P < 0.001$) was determined by one-way ANOVA (*C*, *D*, and *F*), two-way ANOVA (*E*, *F*, *G*, and *H*) for fresh isolates ($N = 4$) and cultured cells ($N = 3$).

demonstrated senescence-associated characteristics of β-gal^{+} and increased cell area coincident with oxidative stress from culture in 21% O_2 (*Figures 2H*; ***$P < 0.001$). The majority of CICs from freshly isolated or 1% O_2 culture were Lin28A^{S+}/β-gal^{-} (68.65 ± 14.8% and 64.83 ± 19.9%, respectively). In contrast, a majority of CICs (64.9 ± 6.9%) from 21% O_2 cultures were Lin28A^{S+}/β-gal^{+}. CIC surface area consistently increases with oxidative stress from culture conditions (*Figure 2I*; **$P < 0.01$). Comparison of Lin28A^{S+}/β-gal^{+} vs. Lin28A^{S+}/β-gal^{-} shows larger cell area whether in fresh (1328 ± 459.8 μm^2 vs. 487.7 ± 221.4 μm^2), 1% O_2 (2167 ± 322.8 μm^2 vs. 767.6 ± 147.6 μm^2), or 21% O_2 (2571 ± 18.32 μm^2 vs. 824.3 ± 63.93 μm^2). The causal role for oxidative stress promoting Lin28A^{S+} was also demonstrated in the total unfractionated CIC population treated with H_2O_2 (see Supplementary material online, *Figure S4*).

Additional analyses were undertaken to delineate whether acquisition of senescence characteristics of β-gal^{+} and/or cell area enlargement influence Lin28A^{S+}. Lin28A^{S-}/β-gal^{+} CICs were absent from freshly isolated CICs with an increasing per cent of Lin28A^{S+}/β-gal^{+} CICs in 1 and 21% O_2 culture (5.3 ± 1.9% and 15.3 ± 2.0%, respectively; see Supplementary material online, *Figure S5A*; ***$P < 0.001$). Lin28A^{S-}/β-gal^{+} CICs exhibit dramatic increases in surface area compared with Lin28A^{S-}/β-gal^{-} in both 1% O_2 (1645 ± 191.9 μm^2 vs. 533.1 ± 25.8 μm^2) and 21% O_2 (1977 ± 53.62 μm^2 vs. 613.6 ± 29.14 μm^2; see Supplementary material online, *Figure S5B*; ***$P < 0.001$).

In reviewing β-gal^{+} CICs, results show fresh isolates are rare for Lin28A^{S+} and are less frequently positive, compared with Lin28A^{S-} in 1% O_2 (84.23 ± 3.06% vs. 15.51 ± 3.284%) and 21% O_2 (89.38 ± 1.412% vs. 10.28 ± 1.363%; see Supplementary material online, *Figure 5C*; ***$P < 0.001$). Surface area of β-gal^{+} CICs are slightly larger when also positive for Lin28A^{S+}, compared with Lin28A^{S-}, in 1% O_2 (2172 ± 185.6 μm^2 vs. 1651 ± 177.4 μm^2) and 21% O_2 (2523 ± 48.58 μm^2 vs. 2011 ± 43.37 μm^2; see Supplementary material online, *Figure S5D*; *$P < 0.05$). In reviewing β-gal^{-} CICs, results show CICs are rarely Lin28A^{S+} in fresh isolates (4.138 ± 0.6901%) and CICs at Passage 2 and expanded in 1% (2.147 ± 0.5949%) oxygen and 21% (1.515 ± 0.0834%) oxygen (see Supplementary material online, *Figure S5E*; ***$P < 0.001$). Surface area of β-gal^{-} CICs are consistently small regardless of being positive for Lin28A^{S+}, compared with Lin28A^{S-}, in fresh isolates (669.2 ± 121.3 μm^2 vs. 325.1 ± 4.102 μm^2), 1% O_2 (615.4 ± 29.52 μm^2 vs. 533.3 ± 25.18 μm^2 and 21% O_2 (858.8 ± 63.29 μm^2 vs. 778.9 ± 95.33 μm^2; see Supplementary material online, *Figure S5F*; **$P < 0.01$).

Collectively, these results demonstrate acquisition of Lin28A^{S+} in response to oxidative stress that correlates with senescence-associated characteristics of β-gal^{+} and cell area enlargement. Conversely,

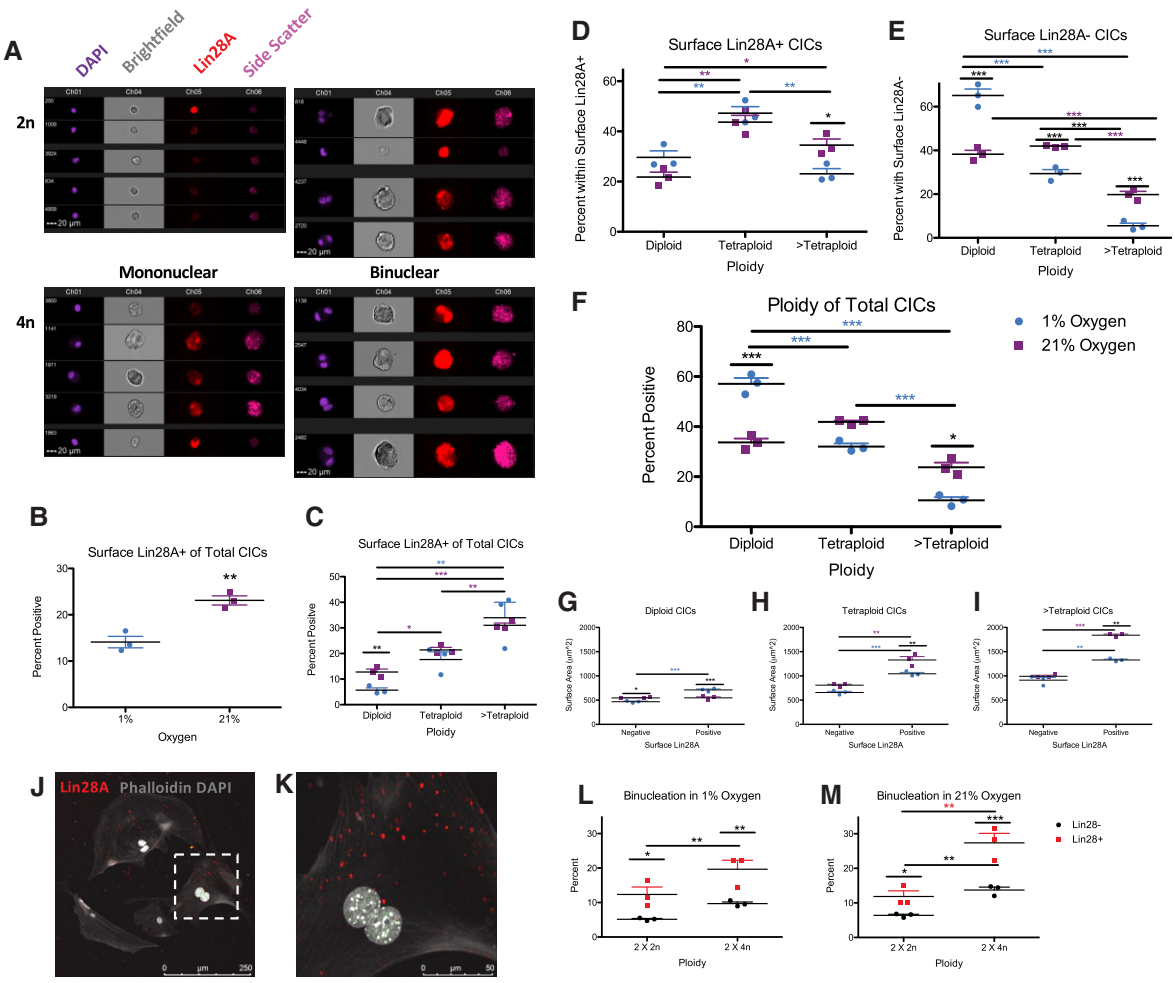

Figure 3 Diploid content favoured by low oxidative stress conditions tracks with CIC phenotypes of Lin28A^{S-} and small size. (*A*) Amnis ImageStream flow cytometry was used to identify and count FVB total CICs for DAPI (Ch01), Brightfield (Ch04), Lin28A^{S} (Ch05), side scatter (Ch06), organized as mononuclear diploid (top left), binucleated diploid (top right) mononuclear tetraploid (bottom left), binucleated tetraploid (bottom right). (*B*) The frequency of Lin28A^{S+} CICs is significantly increased in higher O_2 culture. (*C*) Lin28A^{S+} of total CIC expression is correlated with increased polyploidization. (*D*) Lin28A^{S+} CICs is correlated with increased polyploidization. (*E*) Lin28A^{S-} is correlated with diploid CICs. (*F*) The total CIC population is significantly correlated with increased polyploidization in higher O_2 culture. (*G*) Diploid CICs are consistently small in cell size, regardless of Lin28A^{S} or O_2 culture. (*H*) Tetraploid CICs are of increased size, particularly when Lin28A^{S+}, regardless of O_2 culture. (*I*) >Tetraploid CICs are of increased size, particularly when Lin28A^{S+}, regardless of O_2 culture. (*J*) Total CICs demonstrate binucleation and Lin28A^{S+}, as shown by immunohistochemistry. (*K*) Zoom in region of interest demonstrating binucleation and Lin28A^{S+}. (*L*) Binucleation increases in Lin28A^{S+}, compared with Lin28A^{S-} CICs, in 1% O_2. (*M*) Binucleation increases in Lin28A^{S+}, compared with Lin28A^{S-} CICs, in 21% O_2. Statistical significance (*$P < 0.05$, **$P < 0.01$, ***$P < 0.001$) was determined by *t*-test (*B*), two-way ANOVA (*C–I*, *L*, and *M*) for cultured cells ($N = 3$).

Lin28A^{S-} CICs exhibit diminished senescence-associated characteristics. Therefore, Lin28A^{S+} expression serves as a marker of CIC senescence.

3.3 Diploid content favoured by low oxidative stress conditions tracks with CIC phenotypes of Lin28A^{S-} and small size

Cellular polyploidization is influenced by environmental stress, can alter cell cycle progression, and has been linked to senescence.[33–38] Since Lin28A^{S+} in CICs correlates with oxidative stress and senescence markers (*Figures 1* and *2*), polyploidization was evaluated as an additional phenotype acquired with Lin28A^{S+}. Cellular DNA content was determined using DAPI stain in conjunction with Lin28A^{S+} using Amnis ImageStream (*Figure 3A*, see Supplementary material online, *Figure S6*). Consistent with previous results (*Figure 2*), Lin28A^{S+} was prevalent in 21%, compared with 1% O_2 (23.1 ± 1.0% vs. 14.1 ± 1.3%) in the total CIC population (*Figure 3B*; **$P < 0.01$). Increased ploidy level correlated with Lin28A^{S+} CIC cells in both 1% O_2 and 21% O_2 (*Figure 3C*; *$P <$ 0.005). Polyploidization of Lin28A^{S+} CICs correlates with higher oxidative stress in culture conditions of 21% O_2 compared with 1% O_2 (*Figure 3D*; *$P < 0.05$; see Supplementary material online, *Figure S7A*), whereas diploid CICs were more frequent in 1% O_2 compared with 21% O_2. Furthermore, diploid CICs were predominantly Lin28A^{S-} in

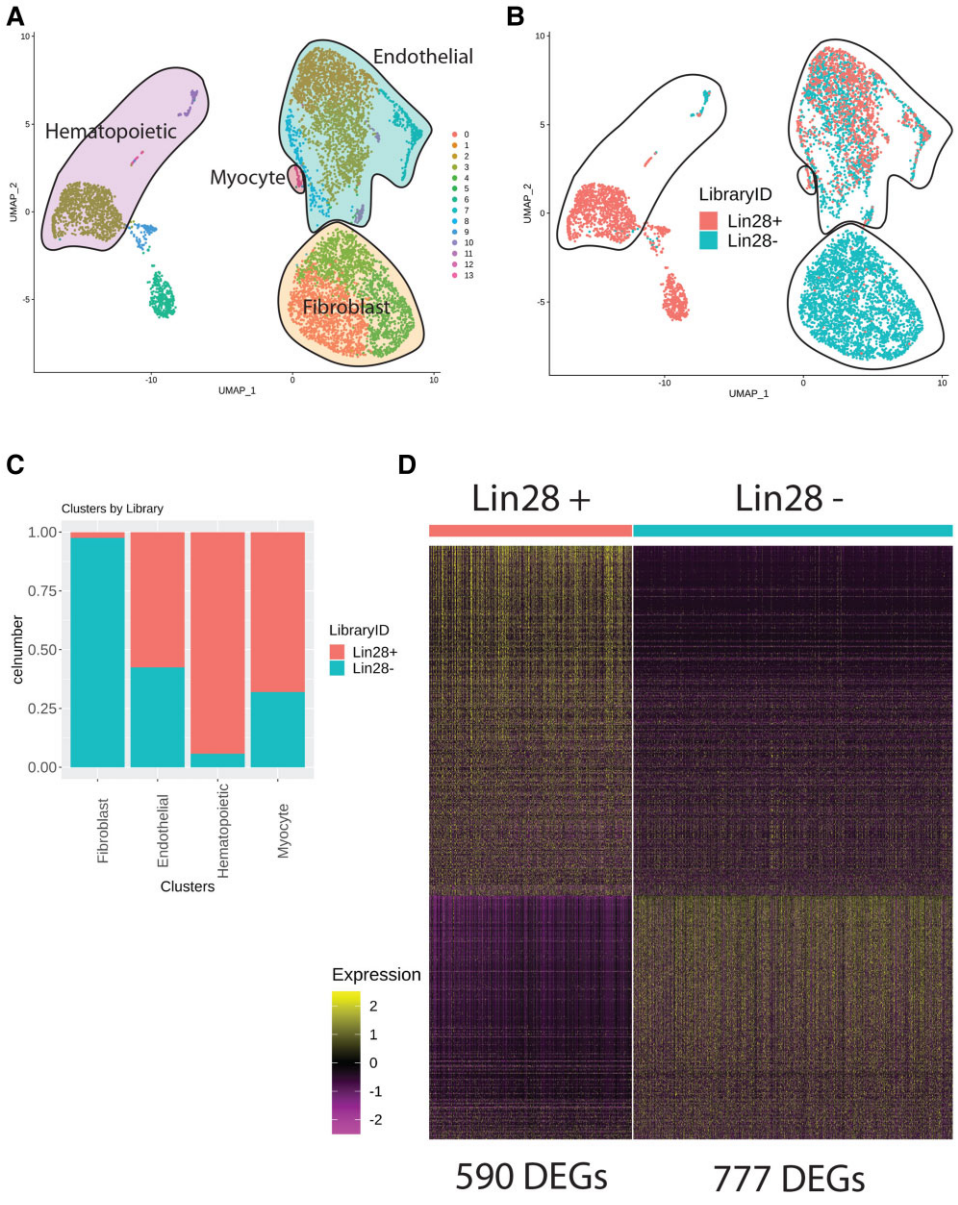

Figure 4 Lin28A^{S+} CICs are predominantly endothelial and haematopoietic lineage. UMAP projection of cardiac interstitial Lin28$^{S+/-}$ colour-coded according to (*A*) unsupervised clustering of gene signatures and (*B*) as derived from either surface presence of Lin28. (*C*) Cell contributions of Lin28$^{S+/-}$ normalized to input of each main cell type as shown in UMAP (*A* and *B*). (*D*) Heatmap representing the differential expressed genes from Lin28$^{S+/-}$ populations.

1% O_2 with higher polyploid content associated with Lin28A^{S-} CICs in 21% O_2 (*Figure 3E*; ***$P < 0.001$; see Supplementary material online, *Figure S7B*). While diploid CICs were the majority population in 1% O_2 (57.1 ± 2.3%), polyploid CICs prevail in 21% O_2 (66.33 ± 1.56%) (*Figure 3F*; *$P < 0.05$). Diploid content correlates with smaller surface area relative to tetraploid CICs regardless of surface Lin28A expression or culture O_2 level (*Figure 3F* and *G*; *$P < 0.05$). Although larger overall, subsets of tetraploid CICs segregate based upon surface Lin28A expression with Lin28A^{S-} cells smaller than their Lin28A^{S+} counterparts (*Figure 3H*; **$P < 0.01$). However, greater than tetraploid content results in the largest surface area regardless of surface Lin28A expression or culture conditions (*Figure 3I*; **$P < 0.01$). Taken together, these results demonstrate that diploid CICs are favoured under culture conditions of low oxidative stress and display a phenotype of Lin28A^{S-} and relatively small cell area.

3.4 Binucleation correlates with Lin28A^{S+} CICs

Nucleation level was determined as part of understanding CIC ploidy status, since polyploidy occurs in both mononuclear and multinuclear cells.[8] Binucleation is more frequently present in polyploid Lin28A^{S+}

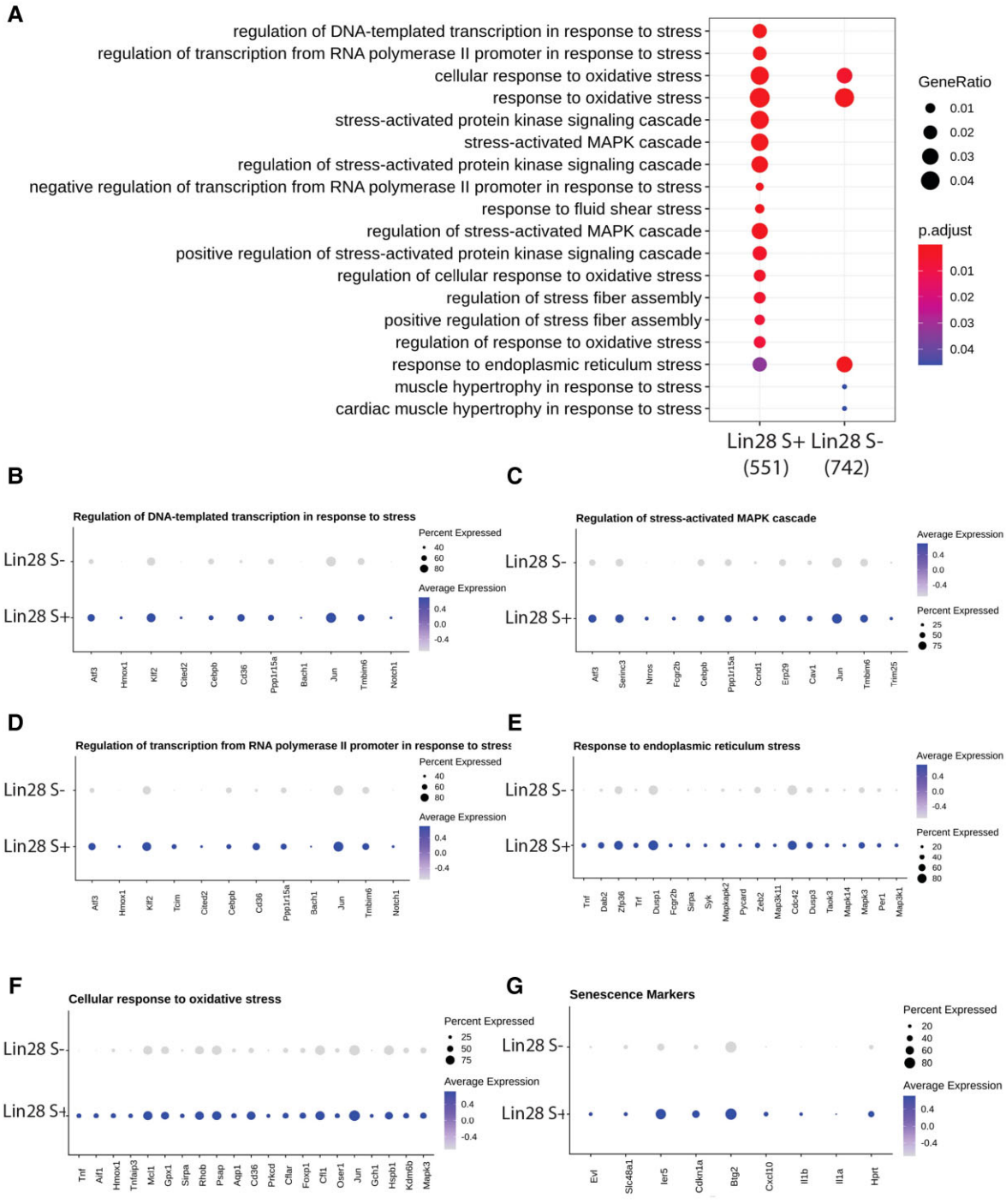

Figure 5 Lin28A^{S+} CICs up-regulate gene markers demonstrating a stress response. (*A*) GO terms results from GO analysis annotated by Biological Process. Circle diameter represents the gene ratio from the 551/742 DEGs being expressed in the Lin28$^{S+/-}$ cells, while significance level is colour-coded according to heatmap scale. Dot plot representing expression of gene targets of stress-associated GO terms (*B*) regulation of DNA-templated transcription in response to stress, (*C*) regulation of stress-activated MAPK cascade, (*D*) regulation of transcription from RNA polymerase II promoter in response to stress, (*E*) response to endoplasmic reticulum stress, and (*F*) cellular response to oxidative stress in both Lin28$^{S+/-}$ populations. (*G*) Senescence markers up-regulated in Lin28$^{S+/-}$ cells. Circle diameter represents the percentage of cells expressing a particular gene, while normalized average expression is represented by colour intensity.

compared with Lin28A^{S-} CICs in 1% O_2 cultures (32.0 ± 3.7% vs. 14.8 ± 0.65%, respectively; *Figure 3L*; *$P < 0.05$). Similar preponderance of polyploid Lin28A^{S+} vs. Lin28A^{S-} CICs was present in 21% O_2 cultures (39.2 ± 1.35% and 20.1 ± 0.73%, respectively; *Figure 3M*; *$P < 0.05$). Thus, multinucleation is more likely when Lin28A is expressed on the surface of polyploid CICs.

3.5 Polyploidization of CICs occurs in response to chronic oxidative stress

Causality of oxidative stress conditions to promote diploid to tetraploid conversion was assessed by serial passaging of CICs in either 1 or 21% oxygen. Freshly isolated CIC stained for DNA content and viability are evenly split between diploid or tetraploid live cells. This 50/50 percentage split between diploid and tetraploid CICs was maintained in 1% O_2 for up to 10 sequential passages. In contrast, ploidy shifted to almost exclusively tetraploid CICs when subjected to the same passaging protocol in 21% O_2 (see Supplementary material online, *Figure S8A*; $*P < 0.05$, see Supplementary material online, *Table S1*). Cytosolic ROS measured at Passage 2 was significantly increased in 21% O_2 compared with 1% O_2 (298.8 ± 25.1 RFU vs. 230.5 ± 5.6 RFU; see Supplementary material online, *Figure S8B*; $*P < 0.05$). Ratio of cytosolic ROS to reactive nitrogen species was similarly elevated in the 21% O_2 compared with 1% O_2 (3167 ± 640.4 RFU vs. 1702 ± 58.09 RFU; see Supplementary material online, *Figure S8C*). These results demonstrate polyploidization as a cellular response to chronic oxidative stress.

3.6 Lin28A^{S+} CICs are predominantly endothelial and haematopoietic lineage

Single-cell RNA-Seq evaluated phenotypic differences of CICs based upon surface Lin28 expression presence (Lin28A^{S+}) or absence (Lin28A^{S-}; see Supplementary material online, *Figures S9–S11*). Dimensionality reduction and unsupervised clustering revealed 14 clusters segregated according to transcriptional phenotype (see Supplementary material online, *Figures S10 and S11*). Canonical cell markers identified four main cell types in the aggregated libraries: fibroblast (Clusters 0, 4, and 5), endothelial (Clusters 1, 2, 7, 11, and 13), haematopoietic (Clusters 3, 10, and 13), and myocyte (Cluster 12; *Figure 4A* and see Supplementary material online, *Figure S12*). Clusters 6, 8, and 9 did not express markers of the main four cell types. However, these clusters appeared transcriptionally like haematopoietic (Clusters 6 and 9) and endothelial (Cluster 8), consistent with the dimensionality reduction results. The similarity was verified by cross-referencing the transcriptional profile with the reference single-cell transcriptome atlas *Tabula muris*[53] (see Supplementary material online, *Figure S13*). Normalization to input revealed fibroblast depletion in the Lin28A^{S+} population with an enrichment for endothelial and haematopoietic cell times (*Figure 4B* and *C*). Lin28A^{S+} were predominant in Clusters 6, 8, and 9 consistent with cell annotation analysis (see Supplementary material online, *Figure S14*). Differential expression analysis revealed transcriptional differences with 590 DEGs identified on Lin28A^{S+} and 777 DEGs on Lin28A^{S-} (*Figure 4D*). Together these results confirm inherent differences in both transcriptional phenotypes and cell-type distributions in the cardiac interstitial linked to presence of surface Lin28A.

3.7 Lin28A^{S+} CICs up-regulate gene markers demonstrating a stress response

Differentially expressed genes derived from differential expression analysis were used as input for GO analysis. GO term analysis of biological processes revealed an enrichment of various ontologies associated with cellular stress in Lin28A^{S+} CICs and up-regulated genes overlapping in multiple ontologies, such as Atf3, Hmox1, Klf2, Cited2, Cebpb, Cd36, Bach1, and Jun among others (*Figure 5A–F*). Lin28A^{S+} CICs also demonstrate up-regulated senescence genes (*Figure 5G*). Lin28A^{S+} DEGs demonstrated to be involved in the regulation of DNA-template transcription and RNA polymerase in response to stress, stress-induced activation of MAPK signalling, response to endoplasmic reticulum, and oxidative stress. Collectively these results demonstrate Lin28A^{S+} cells exhibit transcriptional profiles associated with response to cellular stress.

3.8 Oxidative stress-induced phenotypic changes in CICs are inhibited by antioxidant treatment

Beneficial effects of antioxidant treatment to blunt cellular stress as well as cardiomyopathic injury is well documented.[54–57] Among antioxidant compounds, Trolox is a derivative of vitamin E previously used to lower ROS in cultured cells.[54–57] Therefore, Trolox was used to antagonize oxidative stress in cultures of CICs exposed to chronic high oxidative stress of 21% O_2 incubation conditions. CICs were treated with Trolox in a dose-dependent manner (none, 2.5 μM 60 μM 300 μM) immediately upon plating and throughout outgrowth in 21% O_2 until analysis at Passage 2. Surface Lin28A, β-gal, and cell size was analysed using Amnis ImageStream and compared with no treatment baseline (see Supplementary material online, *Table S2*). Frequency of Lin28A^{S+} CICs was reduced after Trolox treatment in a dose-dependent manner (*Figure 6A*; $*P < 0.05$). Similarly, β-gal^{+} CICs were significantly less prevalent after Trolox treatment, also in a dose-dependent manner compared with no treatment baseline (*Figure 6B*; $*P < 0.05$). Double-positive Lin28A^{S+}/β-gal^{+} CICs were also significantly less frequent after Trolox treatment in a dose-dependent manner (*Figure 6C*; $***P < 0.001$). Cell area of surface was significantly decreased for Lin28A^{S+} CICs after Trolox treatment in a dose-dependent manner, but cell area of Lin28A^{S-} CICs was unchanged by Trolox treatment (*Figure 6D*; $*P < 0.05$). Cell area of Lin28A^{S+} responded differently depending upon β-gal activity, with high-dose Trolox promoting smaller cells in β-gal^{-}, whereas β-gal^{+} CICs were consistently larger (*Figure 6E*; $*P < 0.05$). Proliferation rate remained controlled but was consistently higher when treated with Trolox (*Figure 6F*; $*P < 0.05$). Collectively, these results demonstrate inhibition of oxidative stress-mediated changes by Trolox and confirm the parallel relationship between Lin28A^{S+} and senescence-associated characteristics of β-gal^{+} and cell enlargement.

3.9 Trolox increases diploid population and antagonizes conversion to higher ploidy

Polyploidzation is another hallmark of cellular response to stress and senescence,[33–38] so additional studies were performed to assess the impact of Trolox upon ploidy state of CICs in relation to surface Lin28A expression when cultured in 21% O_2 (see Supplementary material online, *Table S3*). Diploid CICs comprise a significantly higher per cent of the total population with Trolox treatment in a dose-dependent manner (*Figure 7A*; $*P < 0.05$). Trolox treatment reduced the frequency of Lin28A^{S+} in a dose-dependent manner (*Figure 7B*, see Supplementary material online, *Figure S15 and Table S2*) demonstrating antagonism of cellular stress. Lin28A^{S+} expression corresponds with increased presence of polyploidy which was reduced by Trolox treatment in a dose-dependent manner (*Figure 7C*; $*P < 0.05$). Cell size of Lin28A^{S+} CICs correlated with both higher ploidy and larger size, regardless of Trolox dosing (*Figure 7D*; $*P < 0.05$). Lin28A^{S-} CICs exhibit significantly higher frequency of diploid CICs, with a low percentage of polyploidy resulting from Trolox treatment in a dose-dependent manner (*Figure 7E*; $*P < 0.05$). Cell size of Lin28A^{S-} CICs are smaller than Lin28A^{S+} CICs within each ploidy group

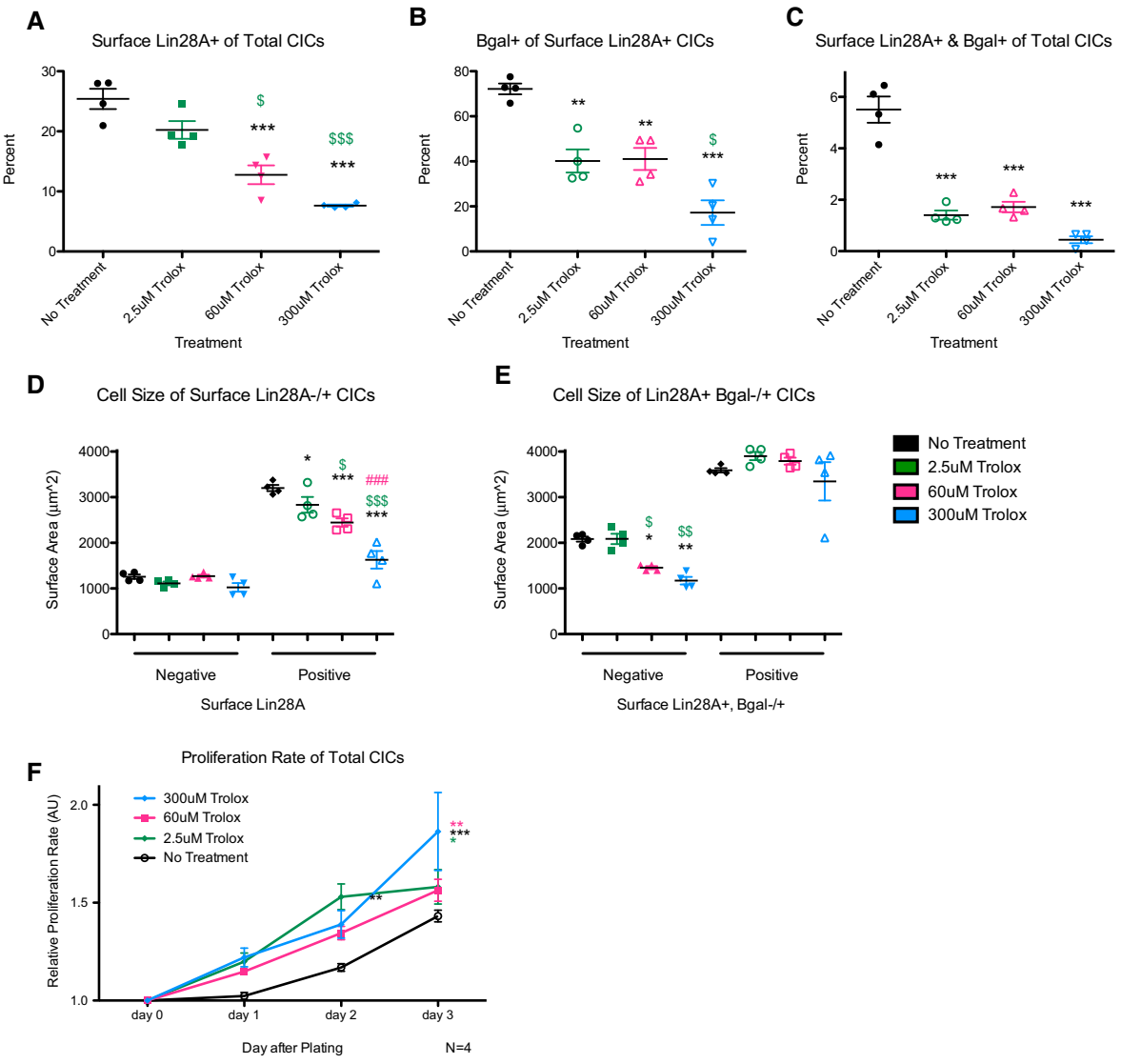

Figure 6 Oxidative stress-induced phenotypic changes in CICs inhibited by antioxidant treatment. (*A*) The frequency of Lin28A^{S+} expression in total CICs cultured in 21% O_2 is significantly decreased when treated with Trolox. (*B*) The frequency of β-gal^{+} expression in total CICs cultured in 21% O_2 is significantly decreased when treated with Trolox. (*C*) The frequency of Lin28^{S+}/β-gal^{+} expression in total CICs cultured in 21% O_2 is significantly decreased when treated with Trolox. (*D*) The size of Lin28^{S+} CICs is reduced by Trolox treatment in a dose-dependent manner. (*E*) The size of Lin28^{S+}/β-gal^{+} CICs is reduced by Trolox treatment in a dose-dependent manner. (*F*) Proliferation rate is higher in total CICs treated with Trolox in a dose-dependent manner. Statistical significance (*$P < 0.05$, **$P < 0.01$, ***$P < 0.001$) was determined by one-way ANOVA (*A*–*F*) for all groups ($N = 4$).

and are consistent in size for each ploidy group, regardless of Trolox dosing treatment (*Figure 7F*; *$P < 0.05$).

4. Discussion

The heterogeneous mixture of CICs includes fibroblasts, endothelial, and haematopoietic cells that serve a critical role in both homeostasis and in response to injury. Preservation of structural integrity and compensation from normal biological ageing to maintain homeostasis comes at the price of decreased tissue compliance, impaired contractile reserve, and replacement fibrosis following accrual of lost myocytes. CICs contribute to regulation of the ageing process through effects upon myocardial structure, interaction with cardiomyocytes, and ongoing contribution to cellular renewal throughout lifespan. Indeed, CIC activity mediates many phenotypic alterations of myocardial structure that typify the ageing heart.[3–5] Although the heart is characterized by barely perceptible myocyte turnover in adulthood, CIC proliferative capacity is retained throughout life even as senescence markers accumulate.[6,7] Understanding regulatory mechanisms influencing CIC proliferation, senescence and polyploidization provides essential insights for ageing cardiomyopathy and reveal strategic interventional approaches to mitigate progression of structural and functional degeneration, perhaps even in favour of prolonging beneficial cellular replacement and tissue repair.

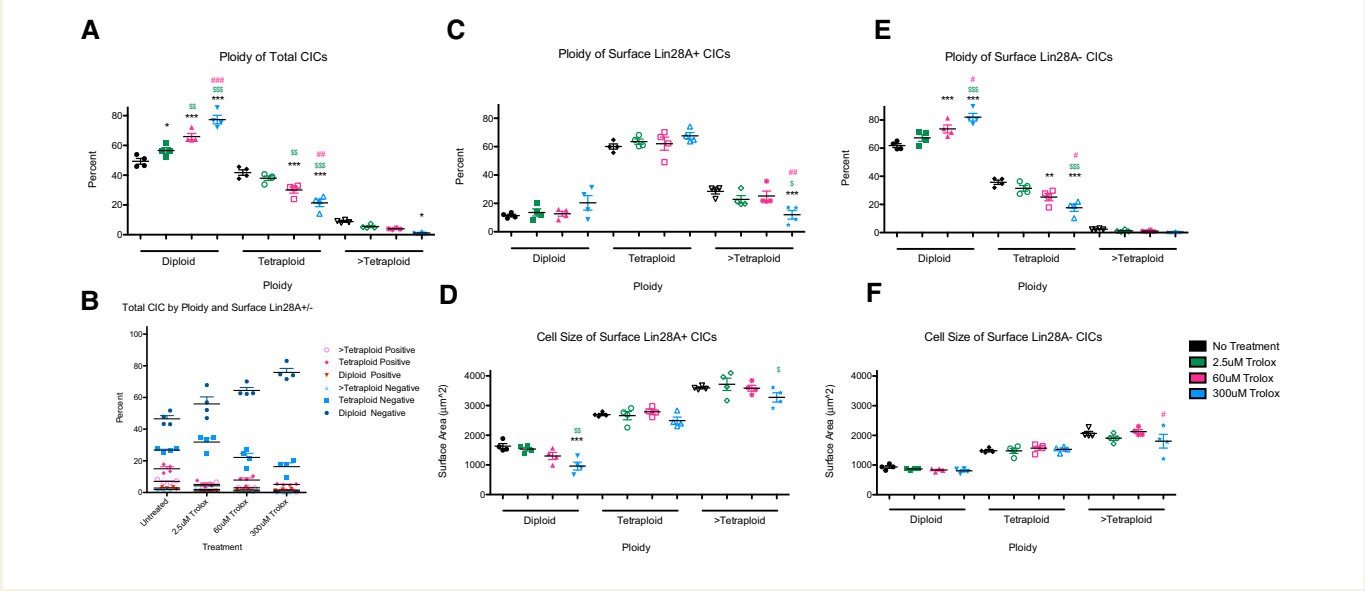

Figure 7 Trolox increases diploid population and antagonizes conversion to higher ploidy. (*A*) The frequency of diploid total CICs cultured in 21% O_2 is significantly increased when treated with Trolox in a dose-dependent manner. (*B*) The frequency of Lin28^{S+} CICs and polyploidization in total CICs cultured in 21% O_2 is significantly decreased when treated with Trolox in a dose-dependent manner. (*C*) The ploidy of Lin28^{S+} CICs cultured in 21% O_2 is unchanged with Trolox. (*D*) The size of Lin28^{S+} CICs treated with Trolox in a dose-dependent manner is significantly larger based on ploidy content. (*E*) The frequency of diploid Lin28^{S-} CICs cultured in 21% O_2 is significantly increased when treated with Trolox in a dose-dependent manner. (*F*) The size of Lin28^{S-} CICs treated with Trolox in a dose-dependent manner is relatively unchanged based on ploidy content. Statistical significance (*$P < 0.05$, **$P < 0.01$, ***$P < 0.001$) was determined by one-way ANOVA (*A*, *C–F*) for all groups ($N = 4$).

Biological ageing impacts both the structural integrity and the functional capacity of the myocardium. Previous studies have shown Lin28 up-regulation in cardiomyocytes to increase susceptibility to apoptosis.[28] In these studies, Lin28A also increased in response to cardiac ageing (*Figure 1*). Molecular signalling studies have affiliated Lin28A activity with downstream targets of cell cycle regulators (Myc, Ras, cyclins, cyclin-dependent kinases, hmga2, and PI3K-Akt), ribosomal biogenesis, mTOR, and insulin-dependent glycolytic metabolism.[31] Cell cycle, among various processes, becomes de-regulated during ageing.[3–5] CIC activity mediates many phenotypic alterations of the ageing heart,[3–5] with this study identifying Lin28A^{S+} as a marker of oxidative stress leading to senescent markers in CICs that would promote the ageing process.

The ageing heart is particularly impacted by oxidative stress.[58,59] Supplemental O_2 therapy (hyperoxia) is widely used in critical and intensive care settings and associated with lung injury and higher risk for mortality.[60,61] Hyperoxia also induces cardiac inflammation, toxicity, and pathophysiology.[62,63] These reports prompted speculation that standard cell culture of 21% O_2 tension recapitulates hyperoxia stress upon CICs, since physiologic O_2 levels are closer to 5 or 1% in hypoxic niches.[64] In this study, Lin28A^{S+} was identified endogenously in a subpopulation of CICs, which frequency was found to increase in natural ageing and accelerated in response to injury (*Figure 1* and see Supplementary material online, *Figure S2*). Senescence marker p16 was frequency identified in Lin28A^{S+} CICs (*Figure 1*). Intracellular ROS production is an indicator of oxidative stress and is associated with biological ageing,[42–46] polyploidy,[65] senescence, and loss of functional competency.[66] Increased ROS activity in response to oxidative stress impacts myocardial ageing[42–46] and polyploidy[65] undoubtedly negatively impacts myocardial biology, promoting senescence, and loss of functional competency.[66] Consistent with these findings, our results show that oxidative stress, through culturing in 21% O_2, directly increases frequency of Lin28A^{S+} CICs in concert with senescence-associated β-gal$^+$ and increased cell size (*Figure 2*). β-gal$^+$ CICs are larger in size regardless of Lin28A^{S+}, with β-gal$^-$ CICs being significantly smaller. To our knowledge, this is the first study identifying Lin28A^{S+} as a marker of oxidative stress. This finding corroborates our previous study demonstrating human cCICs exhibit increased frequency of senescence when culturing in 21% O_2.[67] Results from this study also demonstrate that senescence markers may be dampened when cultured at physiologic O_2 levels, replicated with 1% O_2.

Oxidative stress also influences ploidy of the CICs. Lin28A^{S+} correlated with increased cellular ploidy content, evident in CICs grown in 1 and 21% O_2. Lin28A^{S-} CICs were mostly diploid in 1% O_2 vs. an even mix of diploid and tetraploid when grown in the 21% oxygen at Passage 2 (*Figure 3*). Serial passaging for 10 splits of CICs in 21% O_2 yields a polyploid population, whereas a consistent mixture of diploid and tetraplopid CICs persists in 1% O_2 (see Supplementary material online, *Figure S8*). Our findings establish CIC polyploidization in response to oxidative stress with additional correlations to increased Lin28A^{S+} and higher ploidy content.

Cardiomyocyte polyploidization occurs during development, ageing, and end-stage cardiomyopathies in conjunction with oxidative stress.[35,68–71] Our group subsequently confirmed prior reports of cardiomyocyte polyploidzation, extending this concept to tetraploidization of murine cCIC population.[8] Polyploidization of CIC remains poorly investigated, and results of the present study advance the field by showing chronic oxidative stress correlates with CIC polyploidization and Lin28A^{S+} (*Figure 3*).

Single-cell RNA-Seq offers unprecedented insights regarding cellular heterogeneity by assessment of nuanced transcriptome variation.

scRNA analyses reveal up-regulation of multiple gene families in Lin28A^{S+} CICs associated with DNA transcription and cellular response to stress, specifically oxidative stress (*Figures* 4 and 5). Fresh isolate Lin28A^{S+} preferentially typifies resident CIC lineage of endothelial rather than fibroblast origin, whereas haematopoietic CICs of extra-cardiac origin are mostly Lin28A^{S+}. The convergence of Lin28A^{S+} with endothelial lineage is consistent with endothelial biology in microenvironments of increased cellular stresses including ROS.[72] Freshly isolated Lin28A^{S+} CICs demonstrate up-regulation of genes associated with senescence-associated secretory protein (SASP) markers Cxcl10, IL1a, IL1b, and substantial up-regulation of DNA damage markers Ier5, Cdkn1a, and Btg2 (*Figure* 6). SASP represents cell and tissue ageing[73] and DNA damage markers Cdkn1a and Btg2 are associated with p21[74] and p53,[75] respectively. The p53-p21 bio-signal cascade, similar to p16 and SA-β-gal^{+}, is consistent with cellular senescence.[76] These markers up-regulated in Lin28A^{S+}, compared with Lin28A^{S-}, CICs demonstrate the importance of Lin28A as a surface marker to identify cellular senescence.

The cardioprotective role of antioxidant therapy via reduction of ROS and oxidative stress is well established,[54–57] consistent with blunting of CIC stress an lowering of Lin28A^{S+} using the antioxidant Trolox, a water-soluble analogue of vitamin E that has been tested *in vivo*. Cardioprotective action of Trolox was reported with enhanced cardiac recovery after ischemia/reperfusion of adult rats,[57] and it is tempting to speculate that this protective action rests in part with biological effects upon CICs. Trolox prompted biological actions upon CICs exposed to oxidative stress including suppression of Lin28A^{S+}, β-gal^{+}, and polyploidization (*Figures* 6 and 7). Trolox treatment also correlates with increased proliferation, consistent with higher frequency of diploid CICs with high Trolox dosing. Biological effects of Trolox upon CICs titrated in a dose-dependent fashion highlighting 'cause and effect' of the compound to inhibit phenotypic markers of stress and senescence. The cellular mechanism of Trolox as a therapeutic treatment for oxidative stress with salutary effects for CICs *in vivo* consequential to ageing or pathological injury should be addressed in future studies.

The CIC population plays a critical role in the structure and function of the myocardium. Lin28A^{S+} expression provides a novel marker for identification of cellular ageing and senescence. Exploiting Lin28A^{S+} expression could yield further insights regarding regulatory pathways responsible for CIC stress and senescence consequential to oxidative stress responses. The identification of Lin28A^{S+} as a marker associated with oxidative stress, senescence, and polyploidization may provide for new therapeutic strategies to maintain a youthful phenotype in the non-myocyte population. Surface markers acquired during cellular stress or ageing such as Lin28A^{S+} are valuable for future investigations intended to either mitigate deterioration of these cells or target senolytic therapies for slowing progression or elimination of myocardial pathogenesis.

Supplementary material

Supplementary material is available at *Cardiovascular Research* online.

Acknowledgement

The authors thank the San Diego State University Flow Cytometry facility for use of flow cytometry equipment. This publication includes data generated at the UC San Diego IGM Genomics Center utilizing an Illumina NovaSeq 6000.

Author contributions

K.B. and M.A.S. conceived the project. K.B., C.E., and D.E. performed CIC isolations. K.B. prepared samples and conducted Amnis flow cytometry, western blot, immunocytochemistry, and immunohistochemistry experiments. F.F. performed CIC isolation and Canto flow cytometry experiment. G.S., D.Y., L.G., and N.G. assisted K.B. with immunocytochemistry and immunohistochemistry experiments. K.B., O.E., and M.M. prepared samples for scRNA-Seq and O.E. performed scRNA-Seq analysis. K.B. and M.A.S. wrote the manuscript and oversaw revisions. All authors provided critical feedback on the manuscript.

Conflicts of interest: None declared.

Funding

This work was supported by the National Heart, Lung and Blood Institute at the National Institutes of Health (R01HL067245 and R01HL105759 to M.A.S.).

Data availability

scRNA-Seq data generated in this study have been uploaded to the Gene Expression Omnibus (GEO) database (GSE186176, released October 22, 2021).

References

1. Benjamin EJ, Muntner P, Alonso A, Bittencourt MS, Callaway CW, Carson AP, Chamberlain AM, Chang AR, Cheng S, Das SR, Delling FN, Djousse L, Elkind MSV, Ferguson JF, Fornage M, Jordan LC, Khan SS, Kissela BM, Knutson KL, Kwan TW, Lackland DT, Lewis TT, Lichtman JH, Longenecker CT, Loop MS, Lutsey PL, Martin SS, Matsushita K, Moran AE, Mussolino ME, O'Flaherty M, Pandey A, Perak AM, Rosamond WD, Roth GA, Sampson UKA, Satou GM, Schroeder EB, Shah SH, Spartano NL, Stokes A, Tirschwell DL, Tsao CW, Turakhia MP, VanWagner LB, Wilkins JT, Wong SS, Virani SS, American Heart Association Council on Epidemiology and Prevention Statistics Committee and Stroke Statistics Subcommittee. Heart disease and stroke statistics-2019 update: a report from the American Heart Association. *Circulation* 2019;**139**:e56–e528.
2. Ko DT, Alter DA, Austin PC, You JJ, Lee DS, Qiu F, Stukel TA, Tu JV. Life expectancy after an index hospitalization for patients with heart failure: a population-based study. *Am Heart J* 2008;**155**:324–331.
3. Gude NA, Broughton KM, Firouzi F, Sussman MA. Cardiac ageing: extrinsic and intrinsic factors in cellular renewal and senescence. *Nat Rev Cardiol* 2018;**15**:523–542.
4. Biernacka A, Frangogiannis NG. Aging and cardiac fibrosis. *Aging Dis* 2011;**2**:158–173.
5. Frangogiannis NG. Cardiac fibrosis: cell biological mechanisms, molecular pathways and therapeutic opportunities. *Mol Aspects Med* 2019;**65**:70–99.
6. Rota M, Goichberg P, Anversa P, Leri A. Aging effects on cardiac progenitor cell physiology. *Compr Physiol* 2015;**5**:1775–1814.
7. Sanada F, Kim J, Czarna A, Chan NY, Signore S, Ogorek B, Isobe K, Wybieralska E, Borghetti G, Pesapane A, Sorrentino A, Mangano E, Cappetta D, Mangiaracina C, Ricciardi M, Cimini M, Ifedigbo E, Perrella MA, Goichberg P, Choi AM, Kajstura J, Hosoda T, Rota M, Anversa P, Leri A. c-Kit-positive cardiac stem cells nested in hypoxic niches are activated by stem cell factor reversing the aging myopathy. *Circ Res* 2014;**114**:41–55.
8. Broughton KM, Khieu T, Nguyen N, Rosa M, Mohsin S, Quijada P, Wang BJ, Echeagaray OH, Kubli DA, Kim T, Firouzi F, Monsanto MM, Gude NA, Adamson RM, Dembitsky WP, Davis ME, Sussman MA. Cardiac interstitial tetraploid cells can escape replicative senescence in rodents but not large mammals. *Commun Biol* 2019;**2**:205.
9. McDaniel K, Hall C, Sato K, Lairmore T, Marzioni M, Glaser S, Meng F, Alpini G. Lin28 and let-7: roles and regulation in liver diseases. *Am J Physiol Gastrointest Liver Physiol* 2016;**310**:G757–G765.
10. Sun Z, Yu H, Zhao J, Tan T, Pan H, Zhu Y, Chen L, Zhang C, Zhang L, Lei A, Xu Y, Bi X, Huang X, Gao B, Wang L, Correia C, Chen M, Sun Q, Feng Y, Shen L, Wu H, Wang J, Shen X, Daley GQ, Li H, Zhang J. LIN28 Coordinately promotes nucleolar/ribosomal functions and represses the 2C-like transcriptional program in pluripotent stem cells. *Protein Cell* 2022;**13**:490–512.
11. Reed R, Magni K. A new view of mRNA export: separating the wheat from the chaff. *Nat Cell Biol* 2001;**3**:E201–E204.
12. Fabbiano F, Corsi J, Gurrieri E, Trevisan C, Notarangelo M, D'Agostino VG. RNA packaging into extracellular vesicles: an orchestra of RNA-binding proteins? *J Extracell Vesicles* 2020;**10**:e12043.

13. Balzer E, Moss EG. Localization of the developmental timing regulator Lin28 to mRNP complexes, P-bodies and stress granules. *RNA Biol* 2007;**4**:16–25.
14. Shyh-Chang N, Daley GQ. Lin28: primal regulator of growth and metabolism in stem cells. *Cell Stem Cell* 2013;**12**:395–406.
15. Hattori A, Buac K, Ito T. Regulation of stem cell self-renewal and oncogenesis by RNA-binding proteins. *Adv Exp Med Biol* 2016;**907**:153–188.
16. Moss EG, Tang L. Conservation of the heterochronic regulator Lin-28, its developmental expression and microRNA complementary sites. *Dev Biol* 2003;**258**:432–442.
17. Piskounova E, Polytarchou C, Thornton JE, LaPierre RJ, Pothoulakis C, Hagan JP, Iliopoulos D, Gregory RI. Lin28A and Lin28B inhibit let-7 microRNA biogenesis by distinct mechanisms. *Cell* 2011;**147**:1066–1079.
18. Rehfeld F, Rohde AM, Nguyen DT, Wulczyn FG. Lin28 and let-7: ancient milestones on the road from pluripotency to neurogenesis. *Cell Tissue Res* 2015;**359**:145–160.
19. Thornton JE, Gregory RI. How does Lin28 let-7 control development and disease? *Trends Cell Biol* 2012;**22**:474–482.
20. Tsialikas J, Romer-Seibert J. LIN28: roles and regulation in development and beyond. *Development* 2015;**142**:2397–2404.
21. Bao MH, Feng X, Zhang YW, Lou XY, Cheng Y, Zhou HH. Let-7 in cardiovascular diseases, heart development and cardiovascular differentiation from stem cells. *Int J Mol Sci* 2013;**14**:23086–23102.
22. Li J, Ren Y, Shi E, Tan Z, Xiong J, Yan L, Jiang X. Inhibition of the Let-7 family microRNAs induces cardioprotection against ischemia-reperfusion injury in diabetic rats. *Ann Thorac Surg* 2016;**102**:829–835.
23. Satoh M, Minami Y, Takahashi Y, Tabuchi T, Nakamura M. A cellular microRNA, let-7i, is a novel biomarker for clinical outcome in patients with dilated cardiomyopathy. *J Card Fail* 2011;**17**:923–929.
24. Seeger T, Xu QF, Muhly-Reinholz M, Fischer A, Kremp EM, Zeiher AM, Dimmeler S. Inhibition of let-7 augments the recruitment of epicardial cells and improves cardiac function after myocardial infarction. *J Mol Cell Cardiol* 2016;**94**:145–152.
25. Tolonen AM, Magga J, Szabo Z, Viitala P, Gao E, Moilanen AM, Ohukainen P, Vainio L, Koch WJ, Kerkela R, Ruskoaho H, Serpi R. Inhibition of Let-7 microRNA attenuates myocardial remodeling and improves cardiac function postinfarction in mice. *Pharmacol Res Perspect* 2014;**2**:e00056.
26. Aguirre A, Montserrat N, Zacchigna S, Nivet E, Hishida T, Krause MN, Kurian L, Ocampo A, Vazquez-Ferrer E, Rodriguez-Esteban C, Kumar S, Moresco JJ, Yates JR III, Campistol JM, Sancho-Martinez I, Giacca M, Izpisua Belmonte JC. In vivo activation of a conserved microRNA program induces mammalian heart regeneration. *Cell Stem Cell* 2014;**15**:589–604.
27. Du Y, Zhang M, Zhao W, Shu Y, Gao M, Zhuang Y, Yang T, Mu W, Li T, Li X, Sun F, Pan Z, Lu Y. Let-7a regulates expression of beta1-adrenoceptors and forms a negative feedback circuit with the beta1-adrenoceptor signaling pathway in chronic ischemic heart failure. *Oncotarget* 2017;**8**:8752–8764.
28. Joshi S, Wei J, Bishopric NH. A cardiac myocyte-restricted Lin28/let-7 regulatory axis promotes hypoxia-mediated apoptosis by inducing the AKT signaling suppressor PIK3IP1. *Biochim Biophys Acta* 2016;**1862**:240–251.
29. Gray C, Li M, Patel R, Reynolds CM, Vickers MH. Let-7 miRNA profiles are associated with the reversal of left ventricular hypertrophy and hypertension in adult male offspring from mothers undernourished during pregnancy after preweaning growth hormone treatment. *Endocrinology* 2014;**155**:4808–4817.
30. Shi F, Yu W, Wang X. Bistable switch in let-7 miRNA biogenesis pathway involving Lin28. *Int J Mol Sci* 2014;**15**:19119–19133.
31. Viswanathan SR, Daley GQ. Lin28: a microRNA regulator with a macro role. *Cell* 2010;**140**:445–449.
32. Anatskaya OV, Vinogradov AE. Genome multiplication as adaptation to tissue survival: evidence from gene expression in mammalian heart and liver. *Genomics* 2007;**89**:70–80.
33. Silva IS, Ghiraldini FG, Veronezi GMB, Mello MLS. Polyploidy and nuclear phenotype characteristics of cardiomyocytes from diabetic adult and normoglycemic aged mice. *Acta Histochem* 2018;**120**:84–94.
34. Herget GW, Neuburger M, Plagwitz R, Adler CP. DNA content, ploidy level and number of nuclei in the human heart after myocardial infarction. *Cardiovasc Res* 1997;**36**:45–51.
35. Yan SM, Guerra S, Finato N, Di Loreto C, Beltrami CA. Changes in DNA content of myocardial cells after cardiac explantation. *Adv Clin Path* 1999;**3**:23–27.
36. Rivello HG, Meckert PC, Vigliano C, Favaloro R, Laguens RP. Cardiac myocyte nuclear size and ploidy status decrease after mechanical support. *Cardiovasc Pathol* 2001;**10**:53–57.
37. McCrann DJ, Nguyen HG, Jones MR, Ravid K. Vascular smooth muscle cell polyploidy: an adaptive or maladaptive response? *J Cell Physiol* 2008;**215**:588–592.
38. Yang D, McCrann DJ, Nguyen H, St Hilaire C, DePinho RA, Jones MR, Ravid K. Increased polyploidy in aortic vascular smooth muscle cells during aging is marked by cellular senescence. *Aging Cell* 2007;**6**:257–260.
39. Gray GA, Toor IS, Castellan R, Crisan M, Meloni M. Resident cells of the myocardium: more than spectators in cardiac injury, repair and regeneration. *Curr Opin Physiol* 2018;**1**:46–51.
40. Feng J, Li Y, Nie Y. Non-cardiomyocytes in heart regeneration. *Curr Drug Targets* 2018;**19**:1077–1086.
41. Firouzi F, Sinha Choudhury S, Broughton K, Salazar A, Bailey B, Sussman MA. Human CardioChimeras: creation of a novel "next-generation" cardiac cell. *J Am Heart Assoc* 2020;**9**:e013452.
42. Li SY, Du M, Dolence EK, Fang CX, Mayer GE, Ceylan-Isik AF, LaCour KH, Yang X, Wilbert CJ, Sreejayan N, Ren J. Aging induces cardiac diastolic dysfunction, oxidative stress, accumulation of advanced glycation endproducts and protein modification. *Aging Cell* 2005;**4**:57–64.
43. Cesselli D, Aleksova A, Sponga S, Cervellin C, Di Loreto C, Tell G, Beltrami AP. Cardiac cell senescence and redox signaling. *Front Cardiovasc Med* 2017;**4**:38.
44. Dai DF, Chen T, Johnson SC, Szeto H, Rabinovitch PS. Cardiac aging: from molecular mechanisms to significance in human health and disease. *Antioxid Redox Signal* 2012;**16**:1492–1526.
45. Dai DF, Chiao YA, Marcinek DJ, Szeto HH, Rabinovitch PS. Mitochondrial oxidative stress in aging and healthspan. *Longev Healthspan* 2014;**3**:6.
46. Di Lisa F, Bernardi P. Mitochondrial function and myocardial aging. A critical analysis of the role of permeability transition. *Cardiovasc Res* 2005;**66**:222–232.
47. Beckman JS, Beckman TW, Chen J, Marshall PA, Freeman BA. Apparent hydroxyl radical production by peroxynitrite: implications for endothelial injury from nitric oxide and superoxide. *Proc Natl Acad Sci U S A* 1990;**87**:1620–1624.
48. Di Meo S, Reed TT, Venditti P, Victor VM. Role of ROS and RNS sources in physiological and pathological conditions. *Oxid Med Cell Longev* 2016;**2016**:1245049.
49. Macosko EZ, Basu A, Satija R, Nemesh J, Shekhar K, Goldman M, Tirosh I, Bialas AR, Kamitaki N, Martersteck EM, Trombetta JJ, Weitz DA, Sanes JR, Shalek AK, Regev A, McCarroll SA. Highly parallel genome-wide expression profiling of individual cells using nanoliter droplets. *Cell* 2015;**161**:1202–1214.
50. Fu R, Gillen AE, Sheridan RM, Tian C, Daya M, Hao Y, Hesselberth JR, Riemondy KA. clustifyr: an R package for automated single-cell RNA sequencing cluster classification. *F1000Res* 2020;**9**:223.
51. Schaum CE, Buckling A, Smirnoff N, Studholme DJ, Yvon-Durocher G. Environmental fluctuations accelerate molecular evolution of thermal tolerance in a marine diatom. *Nat Commun* 2018;**9**:1719.
52. Yu G, Wang LG, Han Y, He QY. Clusterprofiler: an R package for comparing biological themes among gene clusters. *OMICS* 2012;**16**:284–287.
53. Tabula Muris Consortium; Overall coordination; Logistical coordination; Organ collection and processing; Library preparation and sequencing; Computational data analysis; Cell type annotation; Writing group; Supplemental text writing group; Principal investigators. Single-cell transcriptomics of 20 mouse organs creates a Tabula Muris. *Nature* 2018;**562**:367–372.
54. Besse S, Bulteau AL, Boucher F, Riou B, Swynghedauw B, de Leiris J. Antioxidant treatment prevents cardiac protein oxidation after ischemia-reperfusion and improves myocardial function and coronary perfusion in senescent hearts. *J Physiol Pharmacol* 2006;**57**:541–552.
55. Costanzo S, De Curtis A, di Niro V, Olivieri M, Morena M, De Filippo CM, Caradonna E, Krogh V, Serafini M, Pellegrini N, Donati MB, de Gaetano G, Iacoviello L, Polyphemus Observational Study I. Postoperative atrial fibrillation and total dietary antioxidant capacity in patients undergoing cardiac surgery: The Polyphemus Observational Study. *J Thorac Cardiovasc Surg* 2015;**149**:1175–1182.e1.
56. Molyneux CA, Glyn MC, Ward BJ. Oxidative stress and cardiac microvascular structure in ischemia and reperfusion: the protective effect of antioxidant vitamins. *Microvasc Res* 2002;**64**:265–277.
57. Sagach VF, Scrosati M, Fielding J, Rossoni G, Galli C, Visioli F. The water-soluble vitamin E analogue Trolox protects against ischaemia/reperfusion damage in vitro and ex vivo. A comparison with vitamin E. *Pharmacol Res* 2002;**45**:435–439.
58. Liguori I, Russo G, Curcio F, Bulli G, Aran L, Della-Morte D, Gargiulo G, Testa G, Cacciatore F, Bonaduce D, Abete P. Oxidative stress, aging, and diseases. *Clin Interv Aging* 2018;**13**:757–772.
59. Martin-Fernandez B, Gredilla R. Mitochondria and oxidative stress in heart aging. *Age (Dordr)* 2016;**38**:225–238.
60. Janz DR, Hollenbeck RD, Pollock JS, McPherson JA, Rice TW. Hyperoxia is associated with increased mortality in patients treated with mild therapeutic hypothermia after sudden cardiac arrest. *Crit Care Med* 2012;**40**:3135–3139.
61. Kilgannon JH, Jones AE, Parrillo JE, Dellinger RP, Milcarek B, Hunter K, Shapiro NI, Trzeciak S. Emergency Medicine Shock Research Network I. Relationship between supranormal oxygen tension and outcome after resuscitation from cardiac arrest. *Circulation* 2011;**123**:2717–2722.
62. Hafner C, Wu J, Tiboldi A, Hess M, Mitulovic G, Kaun C, Krychtiuk KA, Wojta J, Ullrich R, Tretter EV, Markstaller K, Klein KU. Hyperoxia induces inflammation and cytotoxicity in human adult cardiac myocytes. *Shock* 2017;**47**:436–444.
63. Rodgers JL, Iyer D, Rodgers LE, Vanthenapalli S, Panguluri SK. Impact of hyperoxia on cardiac pathophysiology. *J Cell Physiol* 2019;**234**:12595–12603.
64. Wenger RH, Kurtcuoglu V, Scholz CC, Marti HH, Hoogewijs D. Frequently asked questions in hypoxia research. *Hypoxia (Auckl)* 2015;**3**:35–43.
65. Craige SE, Keaney JF Jr. Polyploidy and dysregulated ROS signaling: the school of hard Nox? *Cell Cycle* 2009;**8**:797.

66. Cianflone E, Torella M, Chimenti C, De Angelis A, Beltrami AP, Urbanek K, Rota M, Torella D. Adult cardiac stem cell aging: a reversible stochastic phenomenon? *Oxid Med Cell Longev* 2019;**2019**:5813147.
67. Korski KI, Kubli DA, Wang BJ, Khalafalla FG, Monsanto MM, Firouzi F, Echeagaray OH, Kim T, Adamson RM, Dembitsky WP, Gustafsson AB, Sussman MA. Hypoxia prevents mitochondrial dysfunction and senescence in human c-kit(+) cardiac progenitor cells. *Stem Cells* 2019;**37**:555–567.
68. Senyo SE, Steinhauser ML, Pizzimenti CL, Yang VK, Cai L, Wang M, Wu TD, Guerquin-Kern JL, Lechene CP, Lee RT. Mammalian heart renewal by pre-existing cardiomyocytes. *Nature* 2013;**493**:433–436.
69. Walsh S, Ponten A, Fleischmann BK, Jovinge S. Cardiomyocyte cell cycle control and growth estimation in vivo—an analysis based on cardiomyocyte nuclei. *Cardiovasc Res* 2010;**86**:365–373.
70. Bensley JG, De Matteo R, Harding R, Black MJ. Three-dimensional direct measurement of cardiomyocyte volume, nuclearity, and ploidy in thick histological sections. *Sci Rep* 2016;**6**:23756.
71. Sukhacheva TV, Chudinovskikh YA, Eremeeva MV, Serov RA. Age-related features of cardiomyocyte ploidy in patients with hypertrophic obstructive cardiomyopathy. *Bull Exp Biol Med* 2015;**159**:95–99.
72. Chang X, Zhao Z, Zhang W, Liu D, Ma C, Zhang T, Meng Q, Yan P, Zou L, Zhang M. Natural antioxidants improve the vulnerability of cardiomyocytes and vascular endothelial cells under stress conditions: a focus on mitochondrial quality control. *Oxid Med Cell Longev* 2021;**2021**:6620677.
73. Basisty N, Kale A, Jeon OH, Kuehnemann C, Payne T, Rao C, Holtz A, Shah S, Sharma V, Ferrucci L, Campisi J, Schilling B. A proteomic atlas of senescence-associated secretomes for aging biomarker development. *PLoS Biol* 2020;**18**:e3000599.
74. Herbig U, Wei W, Dutriaux A, Jobling WA, Sedivy JM. Real-time imaging of transcriptional activation in live cells reveals rapid up-regulation of the cyclin-dependent kinase inhibitor gene CDKN1A in replicative cellular senescence. *Aging Cell* 2003;**2**:295–304.
75. Rouault JP, Falette N, Guehenneux F, Guillot C, Rimokh R, Wang Q, Berthet C, Moyret-Lalle C, Savatier P, Pain B, Shaw P, Berger R, Samarut J, Magaud JP, Ozturk M, Samarut C, Puisieux A. Identification of BTG2, an antiproliferative p53-dependent component of the DNA damage cellular response pathway. *Nat Genet* 1996;**14**:482–486.
76. Mijit M, Caracciolo V, Melillo A, Amicarelli F, Giordano A. Role of p53 in the regulation of cellular senescence. *Biomolecules* 2020;**10**:420.

Translational perspective

Cellular phenotypic changes occurring in response to oxidative stress provides critical insights into biological processes of pathological injury and ageing. Surface Lin28A is novel surface marker of oxidative stress conditions that cause DNA damage and cellular senescence. Accumulation of surface Lin28A was inhibited by antioxidant treatment with lowered indices of cellular stress and senescence, revealing the potential of surface Lin28A as a diagnostic stress marker. Furthermore, therapeutic strategies targeted towards surface Lin28 expression set the stage for next generation senolytics to remove stressed or senescent cells and promote recovery from tissue injury or ageing.